IAEA
International Atomic Energy Agency

INDC(NDS)-0625
Distr. IBA

INDC International Nuclear Data Committee

Summary Report

2nd Research Coordination Meeting

Development of a Reference Database for Particle-Induced Gamma ray Emission (PIGE) Spectroscopy

IAEA Headquarters
Vienna, Austria

8 – 12 October 2012

Prepared by

D. Abriola
IAEA Nuclear Data Section
Vienna, Austria

and

P. Dimitriou
IAEA Nuclear Data Section
Vienna, Austria

and

A. Pedro de Jesus
Centro de Física Nuclear
Lisboa, Portugal

March 2013

Selected INDC documents may be downloaded in electronic form from
http://www-nds.iaea.org/reports-new/indc-reports/
or sent as an e-mail attachment.
Requests for hardcopy or e-mail transmittal should be directed to *services@iaeand.iaea.org*
or to:

Nuclear Data Section
International Atomic Energy Agency
Vienna International Centre
PO Box 100
A-1400 Vienna
Austria

Produced by the IAEA in Austria

March 2013

INDC(NDS)-0625
Distr. IBA

Summary Report

2nd Research Coordination Meeting

Development of a Reference Database for Particle-Induced Gamma ray Emission (PIGE) Spectroscopy

IAEA Headquarters
Vienna, Austria

8 – 12 October 2012

Prepared by

D. Abriola
IAEA Nuclear Data Section
Vienna, Austria

and

P. Dimitriou
IAEA Nuclear Data Section
Vienna, Austria

and

A. Pedro de Jesus
Centro de Física Nuclear
Lisboa, Portugal

Abstract

The Second Research Coordination Meeting (RCM) of the IAEA Coordinated Research Project (CRP) on "Development of a Reference Database for Particle-Induced Gamma-ray Emission (PIGE) Spectroscopy" was held at the IAEA, Vienna, from 8 – 12 October 2012. A summary of the participants' presentations is given as well as background information and recommendations concerning the methodology for the remaining part of the CRP. The feasibility of performing evaluations and developing computer codes to implement the PIGE database was discussed. A list of pending measurements was produced and the monitoring, compilation and assessment of these data was assigned to participants.

March 2013

TABLE OF CONTENTS

1. Introduction

1.1. Background

Particle-Induced Gamma-ray Emission (PIGE) is a powerful analytical technique that exploits the interactions of rapid (~1-10 MeV) charged particles with nuclei located near a sample surface to determine the composition and structure of the surface regions of solids (from ~ 0 to 50 μm) by measurement of characteristic prompt γ-rays. This technique has been used since the early 1960s for different applications ranging from analysis of fission reactor materials to biomedicine, environment, cultural heritage and, more recently, fusion reactor materials. The potential for depth profiling of this technique, with better resolution than other Ion Beam Analysis (IBA) techniques, has long been recognized, however, the implementation has been limited owing to insufficient knowledge of the physical data and lack of suitable user-friendly computer codes for the applications.

Compositions and structures are inferred from measured quantities such as γ-ray spectra or excitation curves, via physical models incorporating the sample structure and the basic physical processes. The primary quantities required to simulate the observed spectra or excitation curves are the stopping power and the cross sections of the interactions involved. Information on stopping powers is largely provided by the considerable body of work of Ziegler and co-workers implemented in the SRIM computer code [1.1].

Although a considerable body of published data exists in the nuclear physics literature for nuclear reaction cross sections with γ-rays in the exit channel, there is no up-to-date, comprehensive compilation specifically dedicated to IBA applications. A number of PIGE cross-section data have already been uploaded to IBANDL (http://www-nds.iaea.org/ibandl) by members of the IBA community. However, there is an overwhelming need for compilation, assessment and evaluation of PIGE data. A preliminary survey of this body of unevaluated experimental data has revealed numerous discrepancies beyond the uncertainty limits reported by the authors, and ion beam analysts are faced with the dilemma of trying to decide which (if any) amongst the divergent cross section data they should use.

This state of affairs has been a preoccupation of the IBA community for many years. Using the experience obtained from developing IBANDL [1.2], and the aid of resources and coordination provided by the IAEA, a concerted effort to improve the situation is under way within this Coordinated Research Project.

1.2. Overall objective

This CRP aims at creating a data library for Ion Beam Analysis that contains reliable and usable data on charged particle γ-ray emission cross sections that will be made freely available to the user community.

1.3. Specific research objectives

To attain this goal a four-pronged approach will be applied:

- identify the most important nuclear reactions for PIGE;
- search the literature and electronic databases and convert relevant nuclear reaction data to the format suitable for use in PIGE simulation programs;
- compare data from different sources and carry out measurements when there are no data available or unresolved discrepancies exist;

- incorporate all measured data into the database, and make them available to the IBA community.

1.4. Expected research output

An electronic database of cross sections for PIGE will be made available on the NDS Web server and on CD. In addition, a comprehensive technical report will be published. The project aims at attaining significant improvements in the knowledge of basic nuclear data for PIGE, thus making this analytical technique as powerful as other IBA methods and even surpassing them in some important cases.

1.5. General information

The project was officially approved in August 2010, and is expected to reach completion in 2014. Three Research Coordination Meetings (RCMs) are planned. In the first RCM [1.3], a detailed work plan was determined and tasks were assigned to participants. In this second RCM, the progress made so far was discussed and further actions to be taken were elaborated. The final RCM near the end of the project will serve to review results and prepare the documentation related to the project.

The second RCM was held at the Agency headquarters in Vienna from 8 to 12 October 2012. The meeting was opened with a welcome address by R. Forrest, Head of the Nuclear Data Section. After short presentations by the participants, the project officer, D. Abriola, outlined the main objective of the meeting as to discuss and summarize the progress made in the measurements, compilation and evaluation of existing data, evaluation of the data format and database design, with a view to the Project's final goal of obtaining a reference database for Particle Induced Gamma-ray Emission (PIGE) Spectroscopy. A. Gurbich was elected chairman and A. Pedro de Jesus agreed to serve as rapporteur for the meeting. The preliminary agenda was adopted without changes (Annex A). The list of participants can be found in Annex B.

The meeting continued with participants' presentations, discussions of both the work carried out and pending, assignment of data assessments to participants and identification of the specific needs for measurements and codes. The last day was devoted to drafting and reviewing the summary report, and approving the assigned tasks. The meeting was closed on schedule. Details of the discussions on different relevant matters are presented below.

References:

[1.1] J.F. Ziegler, J.P Biersack, M.D. Ziegler, SRIM The Stopping and Range of Ions in Matter, Lulu Press Co., 2009.

[1.2] Summary Report Third Research Coordination Meeting on Development of a Reference Data Base for Ion Beam Analysis, 27 – 30 April 2009, Vienna, Austria, IAEA Report INDC(NDS)-0555, December 2009.

[1.3] Summary Report First Research Coordination Meeting on Development of a Reference Data Base for Particle-Induced Gamma-ray Emission (PIGE) Spectroscopy, 16 – 20 May 2011, Vienna, Austria, IAEA Report INDC(NDS)-0589, July 2011.

2. Participants' Presentations

2.1. Calibration and thick and thin Al (p,γ) and (p,p'γ) cross sections, A. Pedro de Jesus

2.1.1. Cross Section Measurement.

Table 2.1. List of cross-section measurements performed for the CRP during the past year.

Reaction	Energy Range	Status
$^{25}Mg(p,p'\gamma)^{25}Mg$	1 – 4 MeV	Data Analysis
$^{9}Be(p,\gamma)^{10}B$	0,7 – 1.7 MeV	To be published
$^{23}Na(p,p'\gamma)^{23}Na$	2 – 4 MeV, γ - 440 keV	To be published
$^{23}Na(p,p'\gamma)^{23}Na$	2 – 4 MeV, γ - other	Data Analysis
$^{19}F(p,p'\gamma)^{19}F$	2 – 4 MeV	Data Analysis
$^{19}F(p,\alpha\gamma)^{19}F$	0,5 – 4 MeV	Data Analysis

In relation to cross section measurements, the procedure to normalize cross sections by RBS procacitons scattered by a heavy component of the target was adopted; hence proton spectra were collected at 160° and 140°, simultaneously with the acquisition of gamma-ray spectra. Thin films (<50 μg/cm^2) were evaporated on thin (~50 μg/cm^2) Ag films. Alpha RBS was done to get the atomic ratio between the desired element and silver.
As an example the results for the $^{23}Na(p,p'\gamma)$ ^{23}Na; 2 – 4 MeV, γ - 440 keV measurement are shown in Figure 2.1. Present results (blue) are compared with previous results of the group (red) and of other authors (green). The 25% discrepancy between red and green values persists along the entire energy range between blue and green values. It was suggested that this discrepancy is due to the instability of NaBr, the compound used by the other authors, as Br evaporates readily from the film even at low beam intensities (50 nA).

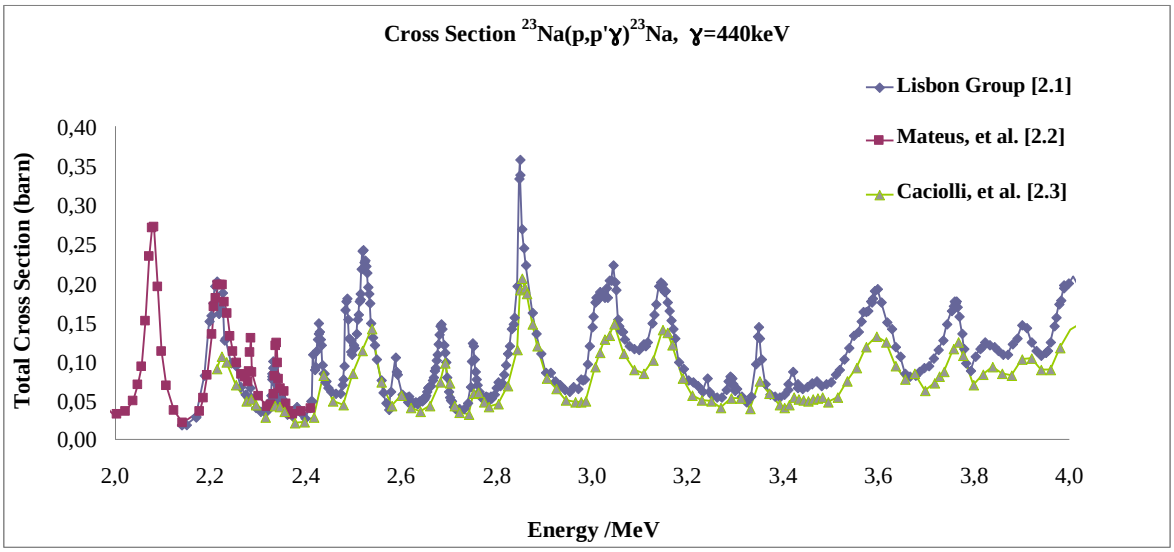

Fig. 2.1. Cross sections of the $^{23}Na(p,p'\gamma)$ reaction using the 440-keV γ line.

It was emphasized that the large amount of spectra and lines to be analysed led to the need to develop automatic spectra analysis (using root – our choice) which caused some delay in data analysis.

2.1.2. Calibration Exercise

Calibration and Thick Al (p,γ) Exercise

Being the Tandem accelerator at the ITN/CFNUL Lab a General Ionex Cockroft-Walton tandetron (3 MV), with a very good high voltage stability (Regulation: +/- 0.1%, High frequency Ripple: 200 V peak to peak (p-p) at 2.5 MV, Low frequency Ripple: 1.0 kV p-p at 2.5 MV, Stability: <1.5 kV at 3.0 MV), it was brought to discussion the approach of calibrating directly the high voltage versus calibrating a deflecting magnet by magnetic resonance. This is especially pertinent due to the fact that two deflecting magnets lead the beam to the reaction chamber and an interplay between them is possible, so that at a given energy more than one value of magnetic field (for each magnet) is possible.

The approach of calibrating directly the high voltage was taken. Thin target nuclear reaction resonances, presented in the table below, were employed to the purpose.

Table 2.2. Thin-target nuclear reaction resonances used for calibration purposes.

Reaction	E_{res}/keV	Γ /keV
$^{19}F(p,a\gamma)^{16}O$	872,11	4,53
$^{19}F(p,a\gamma)^{16}O$	1370,4	11,90
$^{23}Na(p,p'\gamma)^{23}Na$	1645,1	8,00
$^{23}Na(p,p'\gamma)^{23}Na$	1930,7	6,90
$^{24}Mg(p,p'\gamma)^{24}Mg$	2413	
$^{24}Mg(p,p'\gamma)^{24}Mg$	2914	
$^{24}Mg(p,p'\gamma)^{24}Mg$	3660	

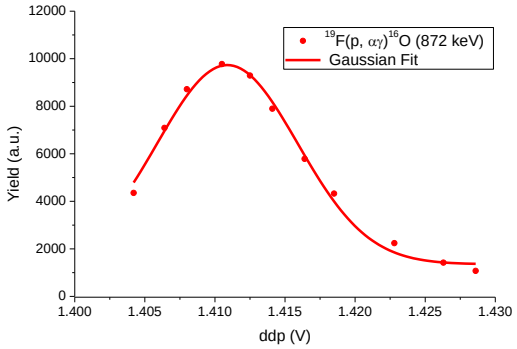

Fig. 2.2. Gaussian fit to 872-keV resonance of $^{19}F(p,\alpha\gamma)^{16}O$ reaction.

The first resonance was used to get the thickness of the target, in order to obtain the experimental resonance energy. A good straight line is obtained as can be seen in Fig. 2.3.

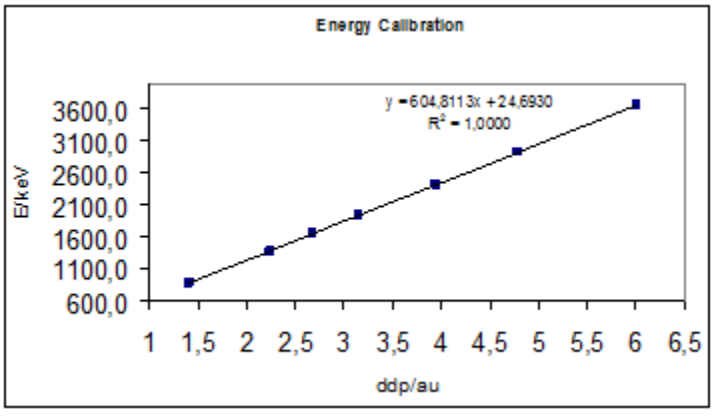

Fig. 2.3. Energy calibration line using the 872 keV resonance of $^{19}F(p, \alpha\gamma)^{16}O$.

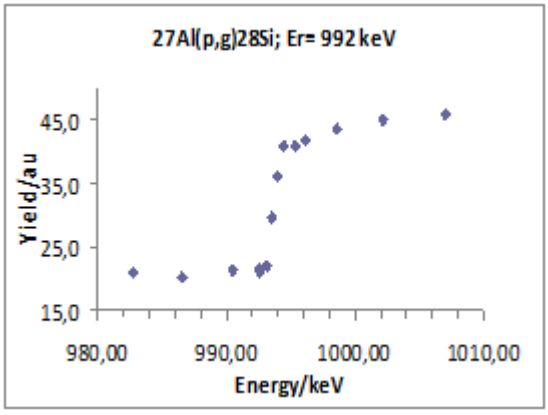

Fig. 2.4. Thick-target yield of $^{27}Al(p, \gamma)^{28}Si$, E_γ = 992 keV line.

2.1.3. Thin and thick Al cross sections – interlaboratory exercise

Using the obtained calibration equation, the resonance of Al (p,γ) at 992 keV, for a thick Al target, is deviated by 2 keV. This deviation gets smaller (~1 keV) if this resonance is included in the calibration procedure.

In relation to energy calibration we may add: from proton spectra pertaining to the ^{23}Na(p,p'γ) ^{23}Na; 2 – 4 MeV, γ - 440 keV measurement, Ag peak areas were extracted. Normalized to the collected charge, these areas follow a $1/E^2$ behaviour (not shown).
For the thick Al (p,γ) exercise the following conditions were used: Target – Thick polished Al foil; Currents – 100-150 nA; Collected Charge –100 μC.

Using the same methodology referred before, gamma-ray and scattered proton spectra were collected simultaneously. The conditions were: Target – Thin Al on thin Ag; Currents – 100 nA; Collected Charge – 40 μC per point. Alpha RBS was not done yet to normalize the results. In arbitrary units, the excitation function is presented below.

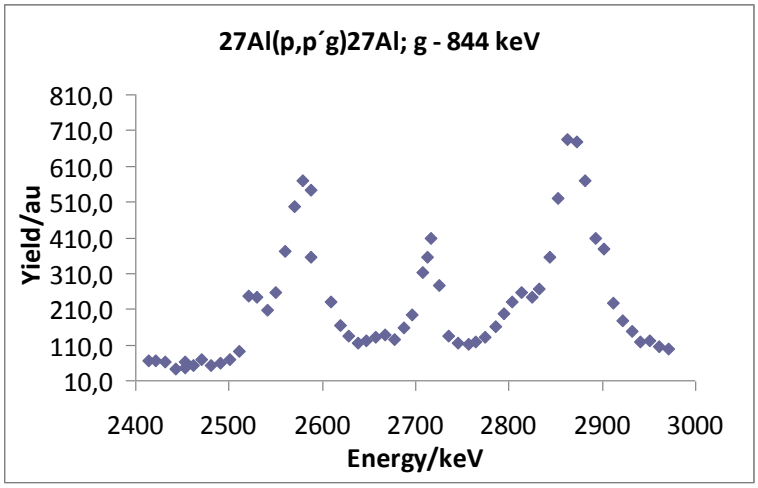

Fig. 2.5. Excitation function of ^{27}Al(p, p'γ), E_γ = 844 keV line.

Finally, the ERYA code and it's capability to analyze mass concentrations of an arbitrary number of elements in a homogeneous sample was demonstrated.

2.2. Gamma ray production cross-sections from deuteron induced nuclear reaction measurements, A.Z. Kiss, et al.

In the context of the present PIGE CRP our group decided to take part in several p-PIGE and d-PIGE thin target cross section measurements. The first task was the energy calibration of our accelerator, followed by the determination of the efficiency curve of the HPGe gamma-ray detector, and finally, to perform gamma-yield measurements and determine the first cross section values as a function of bombarding beam energy. For this experimental programme we chose deuterons as bombarding particles because d-PIGE data are scarce in IBANDL. Silicon nitride was selected as target material, since it has the advantage of being commercially available, and of giving data simultaneously for nitrogen and silicon.

The proton and deuteron beams necessary for calibration and measurement were provided by the 5 MV electrostatic accelerator of ATOMKI. The accelerator has a 90-degree homogeneous field analysing magnet with adjustable energy defining slits before and after it. The magnetic field of

the magnet is measured by a nuclear magnetic resonance (NMR) fluxmeter. After passing through a switching magnet, the beam was transported to the PIGE reaction chamber specifically dedicated to this project and installed to the J30 beam-line. The rather small chamber (with a diameter of 9.5 cm) was insulated from the rest of the beam pipe, but both shared a common vacuum system. The chamber had several diaphragms in its long entrance tube to form a beam of 2 mm diameter and also to eliminate secondary particles, and ended in a long Faraday cup. The accumulated beam charge was measured by an ORTEC 439 Digital Current Integrator. According to the test measurements, the stability of charge measurement was below 1 %..

Gamma-rays were detected by a CANBERRA Model GR4025-7600SL coaxial type HPGe detector (59.5 mm diameter, 170 cm^3 volume, energy resolution 2.3 keV at 1.33 MeV) at an angle of 55° relative to the incident beam direction and at a distance of 9.5 cm between the front face of the detector cryostat and the target.

The detector was surrounded by a lead shield of 5 cm thickness, and additional shields built from lead bricks were applied close to the entrance diaphragms and the Faraday cup to protect the detector against gamma rays originating from them. The inner wall of the target chamber was covered with a copper lining to decrease gamma radiation caused by backscattered particles from the target. We could reduce the gamma radiation background considerably using this arrangement.

The target chamber had an inlet for a particle detector at 135^o to the beam axis. An ORTEC surface barrier detector with a thickness of 300 μm was installed in it. A 3 mm diameter copper collimator was applied before the detector. The solid angle was 5.79 ± 0.02 msr measured by two different methods. This setup was intended to detect the backscattered particles from the target. The novelty of the above experimental arrangement in comparison to our previous measurements is the possibility to measure simultaneously gamma rays and particles from the reactions investigated.

For the energy calibration of the accelerator the resonance at Ep = 991.9 ± 0.1 keV of the $^{27}Al(p,\gamma)^{28}Si$ nuclear reaction was measured on a self-supporting aluminium foil of 750 nm thickness, and the procedure was repeated three months later. From the measurements we concluded that the present calibration is on average 1.9 keV below the reference value with a maximum error of ±1.1 keV. The energy spread between the ¼ and ¾ heights of the step was 1.2 keV which is the average of the energy spreads of the two measurements.

Because we intended to use a deuteron beam, it was necessary to manipulate some of the equipment of the beam transport system to switch from protons to deuterons, which could change the energy calibration of the accelerator by a few keV (as was shown above). To avoid this uncertainty we tried to find a calibration method applicable directly for deuteron beam. One possibility was to detect the neutron threshold using a long counter. The method was checked in the $^7Li(p,n)^7Be$ reaction at the 1880.60 ± 0.07 keV threshold energy. However, turning to deuteron beam our simple long counter detector was completely inapplicable in the $^{16}O(d,n)^{17}F$ reaction (E_{th} = 1829.2±0.6 keV) due to the high number of fast neutrons in the direction of the beam emerging from the d+d reaction caused by the deuteron build up on the slits and diaphragms.

The absolute efficiency determination of the gamma detector was performed in two steps. For the E_γ < 3500 keV energy calibration, radioactive sources ^{133}Ba, ^{56}Co, ^{60}Co, ^{137}Cs and ^{152}Eu were used at the exact position of the target. The sources (except ^{56}Co) had been calibrated beforehand by the Hungarian National Office of Measures. For the E_γ > 3500 keV region, the detector efficiency was determined using gamma cascades from the $^{24}Na(p,\gamma)^{25}Mg$ and

$^{27}Al(p,\gamma)^{28}Si$ reactions at resonance energies 1417 and 992 keV, respectively. To determine the absolute full-energy peak efficiency curve, two different formulas were applied to fit the calibration points, one for energies below 3.5 MeV, and another one for energies up to 10 MeV.

As target, thin silicon nitride films mounted on frames of 5x5 mm^2 were used, which are commercially available**.** The thickness, density and stoichiometry of the Si_3N_4 foil were 200 ± 14 nm, 3.1 g/cm^3 and Si/N = 0.95-1.05, respectively, according to the manufacturer who gave these data for a "low stress nitride" foil. These data were checked by Rutherford backscattering (RBS) measurements using alpha particles in the nuclear microprobe of Atomki and also in our target chamber using backscattered deuterons. The obtained thicknesses were 170 ± 9 and 163 ± 9 nm, respectively. For the sake of completeness, a piece of the silicon nitride foil went under profilometry. The resulting thickness was 212 ± 11 nm. From this result, it was clear that thicknesses calculated from the atoms/cm^2 values were definitely smaller than the thicknesses measured by other methods.

The gamma-ray yield measurements were carried out in two runs. In the first run, the foil was irradiated by deuterons from 2 MeV to 1.05 MeV in 50 keV steps. Three months later, the measurement was continued from 1.8 MeV to 1.05 MeV in 3 steps and from 1.05 MeV to 0.65 MeV in 50 keV steps. The average beam current was around 20 nA in the first run and around 50 nA in the second run. The collected charge varied from 50 to 400 μC to achieve good statistics for all deuteron energy points. Gamma-spectra were evaluated by the FORGAMMA programme package available in the Institute.

From the gamma spectra the yields of the following gamma lines – not disturbed by escape peaks – could be easily determined: 1885, 2297 and 8310 keV energy lines in the case of ^{14}N, while the 1273 and 2028 keV gamma lines in the case of ^{28}Si.

Total cross sections were deduced by two methods: the first one used the thickness, density and stoichiometry data provided by the manufacturer, while the second method used the atom/cm^2 values obtained from the two RBS measurements. The results of both methods in the case of the 8310 keV gamma energy of the $(d,p\gamma_{7\text{-}0})$ transition are shown in Fig. 2.6., where the red dots show the energy dependence of the cross sections calculated with the first method, while the green triangles correspond to cross sections calculated by the second method. The estimated accuracy of the measured points was around 10 %.

To our knowledge only the measurement of van Bebber et al. [2.4] exists in the literature for the 8310 keV gamma line in the $^{14}N(d,p\gamma)^{15}N$ reaction, measured in the 0.5 – 1.5 deuteron energy interval. Comparison with these results showed that the present measurement gives total cross section values by a factor of 1.3 higher than those of van Bebber et al.. The evaluation of the other experimental results is under way.

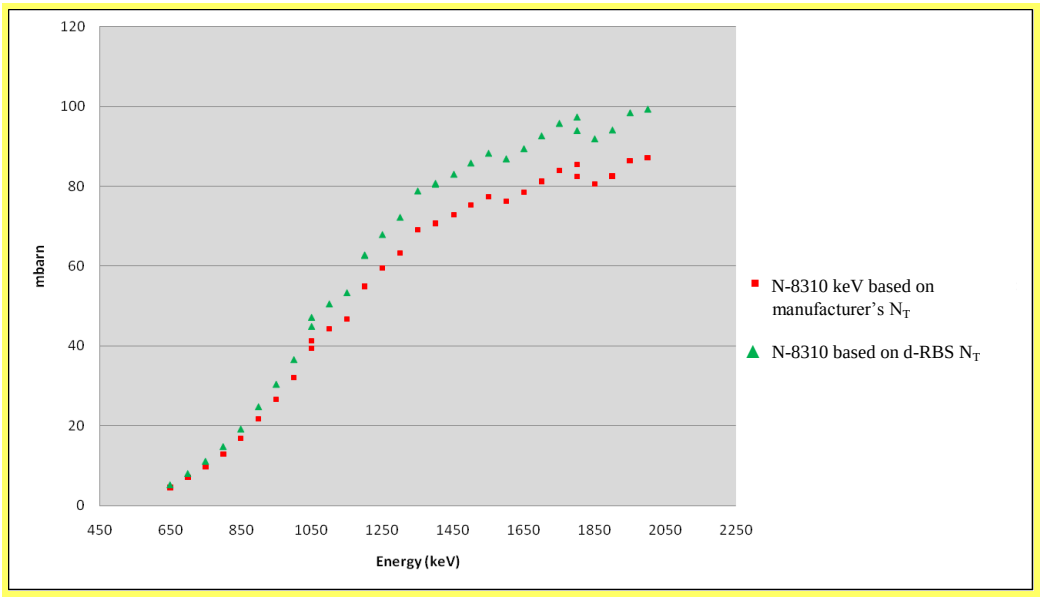

Fig. 2.6. Cross section of the 8310 keV γ-line in the $^{14}N(d,p\gamma_{7-0})^{15}N$ reaction (N_T is target thickness – see Section 3.4)

2.3. Measurements and Literature Survey of Some (p,γ) and (p,αγ) Reactions Important for Ion Beam Analysis, H.-W. Becker

For the depth profiling of light elements as well as for the energy calibration of accelerators and efficiency calibration of detectors the (p,γ) and (p,αγ) resonances play an important role in the ion beam analysis of materials. At the last RCM it was concluded, that the inclusion of cross section or yield data of important reactions as a function of the beam energy in the PIGE database will be most valuable. These data, in addition to the resonance parameters, would allow the user to get an overview of the cross sections and the strength of the various resonances. Moreover, these data directly show the distance between neighboring resonances which is important for applications involving probing of depth.

A vast amount of literature and tabulated data exists from nuclear spectroscopy work, however, these sources often give information such as resonance strengths and other nuclear state information only rather than a complete overview of the variation of the cross section with beam energy.

This latter type of information is important for nuclear astrophysics though, where a complete understanding of the energy dependence of low energy cross section is needed for a sound extrapolation of reaction rates to stellar, i.e. very low energies. These data are published in journals but from a somewhat different viewpoint than that dictated by the needs of material science applications. Therefore, we have started a literature survey in the framework of this contribution to explore which astrophysics data could be valuable for material science and could be included in the PIGE data base. Furthermore we are planning to study, for which reaction new measurements would be desirable.

Several reactions of interest, as mentioned in the report of the last RCM, have been investigated. Three cases are discussed below:

The **$^{27}Al(p,\gamma)^{28}Si$** reaction has been studied extensively in the past, mainly with respect to the properties of the resonances such as resonance energy and decay schemes of the different nuclear states. Thus, it is often used for the energy calibration of accelerators and for an efficiency calibration of detectors. A complete data set for the energy dependence of the reaction yield in

the range between 200 keV and 1150 keV including measurements of the non-resonant cross section has been published. These data represent angle and cascade integrated measurements of the yield using a 4π summing crystal. The resonance strength for the 992 keV resonance deduced in this work is found to agree well with the other sources in literature. Angular distribution coefficients are published as well and show an almost isotropic behavior of the angular distribution.

For the **^{12}C(p,γ)^{13}N** reaction only one measurement of the energy dependence of the cross section at low energies could be found in the literature. Therefore, a new experimental investigation was performed in the last year in collaboration with groups in Notre Dame and Bielefeld. Targets were produced by ion implantation and characterized by Rutherford backscattering spectrometry. The cross section of the reaction was measured in the energy range from 1.05 to 2.55 MeV at detection angles of 0° and 55°. Detailed angular distributions at selected beam energies have been obtained. The data are under analysis and will be published soon.

The **^{15}N(p,αγ)^{12}C** reaction has its widest application in the depth profiling of hydrogen in inverse kinematics with the resonance at an ^{15}N beam energy of 6.4 MeV. Many studies of this reaction can be found in the literature. Some initial data dating back to the 50s of the last century lack experimental resolution to determine the width of the resonance and the cross section on the resonance as well as the non-resonant contribution of the reaction correctly. The latter is of great importance for the measurement of low concentration of hydrogen in a sample. With the extended use of this reaction in inverse kinematics several measurements focusing on aspects of importance to ion beam analysis have been published.. These data are in good agreement and can be included in the IBANDL data base. A comparison of recently published values for the resonance strength and width show a satisfying agreement. Data for the angular distribution of the γ-rays are also available.

Several other reactions such as the ^{19}F(p,αγ)^{16}O or the ^{24}Mg(p,γ)^{25}Al are being investigated. The results will be available to the PIGE data base after an appropriate assessment.

See full presentation for figures and references at http://www-nds.iaea.org/pige/index2.html

2.4. Development of an innovative multipurpose reaction chamber for simultaneous analysis of PIGE, PIXE and RBS, O. Kakuee, et al.

The Van de Graaff Laboratory (VDG lab) of the Nuclear Science and Technology Research Institute (NSTRI) in Tehran has a long history of applying low energy ion beams in various kinds of IBA analysis or fundamental research [2.5-2.9]. In this lab, a 3MV Van de Graaff electrostatic accelerator is used to produce energetic ion beams of H^+, D^+ and He^+ up to 3 MeV. Accurate analysis of various samples is being carried out in seven beamlines equipped either with modern facilities such as a microbeam system (manufactured by Oxford Microbeam Ltd.) and a RBS-channeling system (manufactured by HVE), or with home-made complementary reaction chambers and equipment. The need for accurate measurement of PIGE cross sections in this CRP as well as our desire to introduce an innovative multipurpose reaction chamber for simultaneous analysis of PIGE, PIXE and RBS to the IBA community led us to design and fabricate a reaction chamber.

Design and fabrication of the PIGE reaction chamber and side equipment

The multipurpose PIGE reaction chamber is designed and fabricated for simultaneous measurements of PIGE, PIXE and RBS. The chamber is made of an aluminum alloy with a lining of tin (Sn) to minimize the PIGE background radiation. In fact, for measurement of low concentration elements in sample, minimized background radiation is an important requirement. The following factors were taken into account in the design of the PIGE chamber:

- Maximization of attainable solid angle for measurement of PIGE reaction products with the smallest physical volume of the chamber for rapid evacuation.
- Capability for interchanging the samples without breaking the vacuum.
- Possibility for measuring products of nuclear reaction at scattering angles of 55° and 90° using HPGe detector.
- Equipping the chamber with a surface barrier detector so that RBS analysis and measurement of incident beam current are feasible.
- Equipping the chamber with a Si(Li) detector for measurement of characteristic X-rays at 135°.
- Equipping the chamber with an isolated target holder, which could accommodate 6 samples.

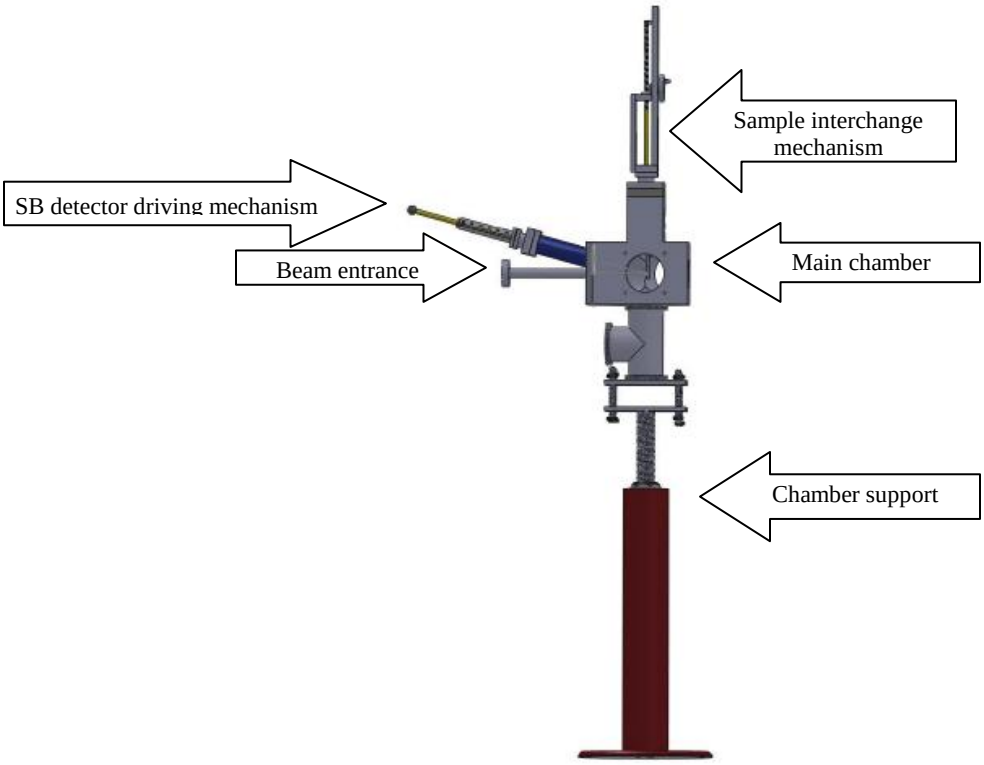

Fig. 2.7. PIGE reaction chamber, its support and sample movement mechanism

Main components of the experimental setup for PIGE analysis as shown in Fig. 2.7 are as follows:

a- PIGE reaction chamber and its ports;
b- Support of the PIGE reaction chamber;
c- Side part for beam entrance and driving mechanism of surface barrier detector;
d- Sample holder and sample interchanging mechanism;
e- Beam current measurement and beam suppression system.

The PIGE reaction chamber is designed and fabricated in such a way that mounting HPGe detectors at 55° and 90°, and mounting Si(Li) detector at 135° can be easily done (Fig. 2.8). Moreover, one could mount a surface barrier detector at 165° with the possibility of changing the detector solid angle without breaking the vacuum. Required ports for connecting vacuum measuring equipment and beam entrance and beam exit accessories to the chamber are foreseen. Side ports for connecting HPGe and Si(Li) detectors could be covered and sealed by the prepared caps using single claw clamps. Moreover, these ports could be readily vacuum-sealed using rings, O-rings and foils such as Kapton.

Fig. 2.8. The established PIGE reaction chamber, sample interchange mechanism and SB detector driving mechanism.

Since beam current in nuclear reaction analysis is considerably high compared to conventional IBA analysis techniques, two options of using Faraday cup and Backscattering spectroscopy are available for beam monitoring. Furthermore, the high current beam could be suppressed by the Faraday cup made of graphite placed at the proper distance from the target-beam intersection point to eliminate the prompt gamma-ray background.

2.5. Cross sections for the $^{14}N(p,p'\gamma)^{14}N$, $^{28}Si(p,p'\gamma)^{28}Si$ and $^{29}Si(p,p'\gamma)^{29}Si$ reactions, J. Raisanen

2.5.1. Summary of presentation

A brief survey of the ion beam equipment available at the University of Helsinki was provided. The survey was followed by detailed description of the procedures employed in the measurements of the relative cross sections for the proton induced nuclear reactions of $^{14}N(p,p'\gamma)^{14}N$, $^{28}Si(p,p'\gamma)^{28}Si$ and $^{29}Si(p,p'\gamma)^{29}Si$ by detecting the gamma-ray lines of 2313 keV, 1779 keV and 1273 keV, respectively.

2.5.2. Experimental

2.5.2.1. Target description

As a target for nitrogen and silicon a thin self-supporting Si_3N_4 membrane obtained from Silson Ltd. was employed. The nominal foil thickness was 100 nm and the window area of the membrane was 5x5 mm^2. The stated membrane thickness is the nominal value, i.e. ± 10%. The additional information concerning the membranes as stated by the manufacturer is as follows.

- Across a single membrane the thickness variation is much better than 1%.
- Membrane roughness is not considerably worse than 5Å.

The membrane composition and areal density were determined accurately by ERDA-measurements allowing absolute cross section determination and fixing of the present relative cross section data on an absolute scale. The membrane areal densities as measured by ERDA are provided in Table 2.3. The selected membrane thickness was chosen to ensure sufficient counting rate, but still so that it can be considered as a thin target in the present experiments.

Table 2.3. Si_3N_4 membrane areal densities and composition as obtained by ERDA.

Element	H	C	N	O	Si
Coverage10^{16} [at/cm^2]	1.34	0.16	36.0	0.84	30.2

2.5.2.2. Irradiation and detection set up

The proton beam was generated by the 5 MV tandem accelerator of the University of Helsinki. Beam energy loss in the membrane is ~2 keV and the initial energy spread was estimated to be less than ± 2.7 keV. The gamma-rays were detected with an 80 cm^3 germanium detector. The proton currents were adjusted to keep the detector count rate fixed and the dead time below 1%. The detector – target distance was 2 cm.

The experimental set-up was described and discussed along with the encountered technical problems. These are mainly related to achieving a sufficiently accurate absolute beam charge collection. The detection angle in the measurements was fixed to 55^o relative to the beam direction. A tantalum collimator (diameter 4 mm) was used in front of the target (Fig. 2.9).

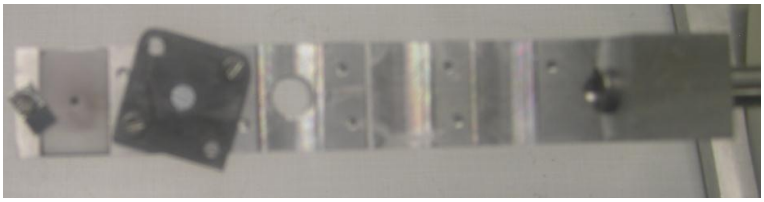

Fig. 2.9. Target collimation.

2.5.3. Measurements and results

The accelerator energy calibration was based on the particle detector of the BepiColombo, SIXS (Solar Intensity X-ray and particle Spectrometer) which has been calibrated by 624.2 keV K-conversion electrons from Cs-137, alpha particles from Pu-238 and Pu-239 sources (energies 5.499/5.4565 MeV and 5.105/5.156 MeV, respectively).

The studied proton energy range includes measurements from 3.6 MeV up to 7 MeV with 100 keV energy steps; in more detail in the range 3.9 MeV to 4.1 with steps of 10 keV. The experimental excitation curves are shown and discussed. The present results are compared with previous data available in the literature and with values found in the various tabulations. As an example the excitation curve for the $^{14}N(p,p'\gamma)^{14}N$ reaction is shown in Fig. 2.10.

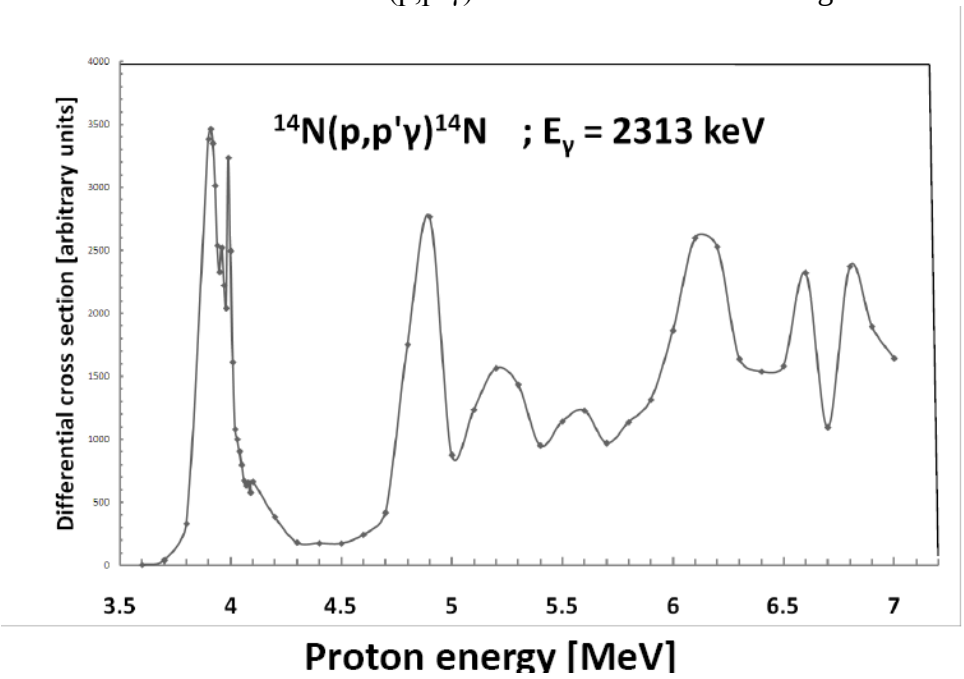

Fig. 2.10. Excitation curve for the reaction $^{14}N(p,p'\gamma)^{14}N$.

2.5.4. Conclusions

The experimental arrangement will be slightly modified to ensure accurate beam current integration so that determination of absolute cross sections is feasible. The employed target proved to be ideal for the present cross section measurements.

2.6. Setting up the HPGe array for PIGE cross-section measurements at LABEC, M. Chiari

The objective of the proposed research is the measurement of the proton induced γ-ray emission cross sections on low-Z nuclei such as Na and Al of specific interest for environmental and cultural heritage applications, for proton beam energy from 2.5 to 4.5 MeV, including the measurement of the angular distributions of the emitted γ-rays at selected angles.

During this first year the activity focused on setting–up the experimental apparatus, performing the energy calibration of the accelerator and obtaining the targets.

To accomplish the measurement of the angular distributions of the proton induced γ-ray emission cross sections, an array of 3 ORTEC HPGe detectors was set-up and coupled to the multi-purpose scattering chamber on the +30° beam line of the Tandetron accelerator at LABEC. The

scattering chamber is equipped with several charged particle detectors for EBS/PESA (165°, 150°, 120° and 30° scattering angles) that can be used to measure the elastic scattering of the beam particles at backward angles for cross-section normalization, and two X-ray detectors, SDD and Si(Li), for PIXE. The scattering chamber is also equipped with a remote controlled multi-sample target holder.
The HPGe detectors are placed at angles of 90°, 45° and 0° (Fig. 2.11) with respect to the beam direction, outside the scattering chamber at about 19-20 cm from the target, in correspondence of stainless steel flanges that have been machined in order to reduce the thickness to 2 mm; note that 2 mm of stainless steel will produce an attenuation of 15% and 10% for 500 keV and 1 MeV energy γ-rays, respectively.
The HPGe detectors (nominal efficiency 25% at 1.33 MeV and energy resolution 2.2 keV FWHM at 1.33 MeV) have been borrowed from the pool of γ-ray detectors of the local GAMMA collaboration group. These detectors were chosen on the basis of the best measured energy resolution and efficiency from preliminary laboratory tests.

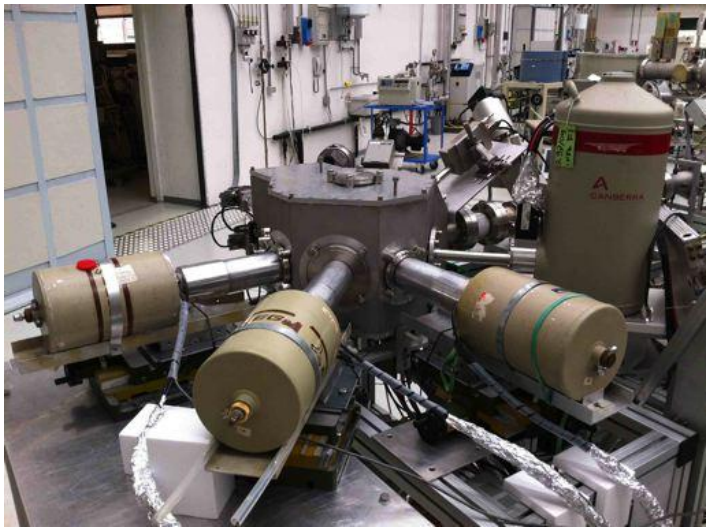

Fig. 2.11. The three HPGe detectors coupled to the multipurpose scattering chamber on the +30° beam line, placed at angles of 0°, 45° and 90° with respect to the incoming beam direction; the two PIXE detectors, a Si(Li) and a SDD are visible as well.

The measurement of the absolute efficiency of the HPGe detectors of the array was carried out using a ^{152}Eu calibration source (activity 370 kBq as per February 2003) mounted on the target holder and placed in the exact position of the target under irradiation. In Fig. 2.12 the final plot with the experimental data and the fitted absolute efficiency curves for each detector is shown.

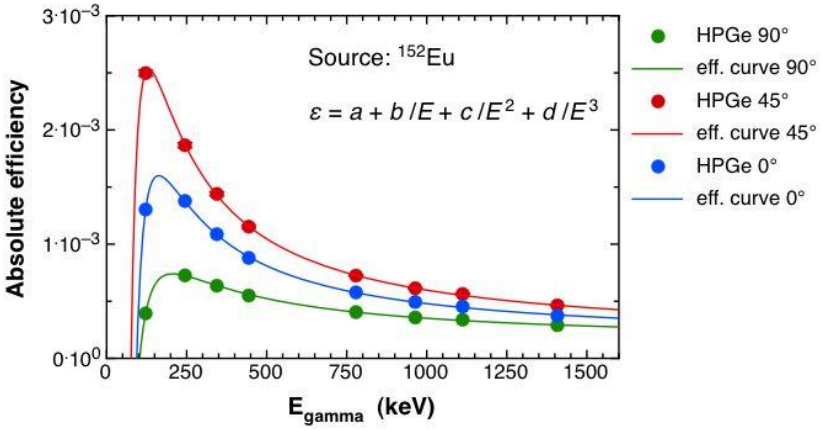

Fig. 2.12. Measured absolute efficiencies for the 3 HPGe detectors of the array together with the fitted curves.

These measurements pointed out a remarkable decrease of the absolute efficiency of the HPGe detector placed at 0° when the Faraday cup (a stainless steel cylinder with inner Ta lining) is kept in its position inside the scattering chamber. To reduce this shielding effect, a new Faraday cup is currently under design, made of highly pure graphite and with a Ta bottom. Moreover, the sample holder structure is also partially reducing the absolute efficiency of the HPGe detector placed at 90°, with respect to the expected values as measured in the laboratory tests. Therefore, a new streamlined sample holder exclusively designed for mounting the frames of the thin targets will be installed in the scattering chamber.

The energy calibration of the HVEE 3 MV Tandetron accelerator at LABEC was accomplished by using resonances at proton beam energies of 991.86 ± 0.03 keV and 1683.57 ± 0.13 keV in the (p,γ) and (p,p′γ) reactions on ^{27}Al, respectively, and of 3470 ± 5 keV and 4808 ± 10 keV in the proton elastic scattering on ^{16}O and ^{12}C, respectively.

The targets used were thick polished Al, thin target of O (a few μg/cm^2 from the oxidation layer of a thin self-supporting Al foil) and thin self-supporting C foil (about 15 μg/cm^2).

The measurements of the γ-rays were carried out with a different detector, i.e. with a 70% efficiency ORTEC HPGe detector placed at 90°, while for the elastically scattered protons the EBS detector (an Hamamatsu 10x10 mm^2 PIN diode) was placed inside the scattering chamber at 150° .

The calibration curve of the terminal voltage of the accelerator, i.e. the relationship between the nominal value, in kV, of the terminal voltage, TV_{nom}, and the measured value, TV_{meas}, was found to be $TV_{meas} = 1.0068 \cdot TV_{nom} - 3.5$ kV. After the calibration, the proton beam energy is known with an uncertainty of ±0.1%.

The targets to be used for the measurement of the proton induced γ-ray emission cross sections will be prepared by ITN in Lisbon thanks to the collaboration of Dr. Micaela Fonseca. Thin film targets of NaCl, NaF and Al (approximately 10-20 μg/cm^2) will be deposited on thin self-supporting Ag (about 50 μg/cm^2). The target thickness and the elemental ratios will be measured by RBS in Lisbon as well. A few cross-section values at selected energies will also be measured again in Lisbon with these new targets, before shipping them to LABEC for an inter-comparison exercise between the two laboratories.

2.7. PIGE measurements at the Ruđer Bošković Institute, I. Bogdanović Radović, et al.

PIGE laboratory activities during the last year can be divided into cross- section measurements and method applications for determination of light element content in minerals and dental alloys. As assigned during the first RCM, PIGE cross sections were measured using a HPGe detector with 20% nominal efficiency placed at 135°. Protons between 1.8 and 3 MeV and with 15 keV energy steps were used. Cross sections for the following reactions were measured:

^{23}Na(p,p'γ)^{23}Na (E_γ = 440 and 1636 keV)
^{23}Na(p,αγ)^{20}Ne (E_γ = 1634 keV)
^{25}Mg(p,p'γ)^{25}Mg (E_γ = 390 and 585 keV)
^{27}Al(p,p'γ)^{27}Al (E_γ = 844 and 1014 keV)
^{27}Al(p,αγ)^{24}Mg (E_γ = 1369 keV)
^{19}F(p,p'γ)^{19}F (E_γ = 110, 197, 1236 and 1349+1357 keV)

Prior to cross section measurements, the accelerator energy calibration was performed using reactions ^{27}Al(p,γ)^{28}Si at E_p=(991.9±0.1) keV for E_γ=1.778 MeV and ^{7}Li(p,n)^{7}Be, threshold at E_p=(1880.7±0.4) keV. It was found that the energy resolution of the beam is 0.1 %.
Thin Micromatter standards deposited on 6.3 μm thin Mylar foils 53.7 μg/cm^2 of NaCl, 54.1 μg/cm^2 of MgF_2 and 55 μg/cm^2 of Al were used for the measurements. For normalization purposes, targets were covered with ~ 4 nm Au. Together with the PIGE spectra, backscattered protons were collected with the SB detector placed at 165°. The absolute HPGe detector efficiency was measured by placing calibrated sources (^{60}Co, ^{137}Cs, ^{133}Ba, ^{152}Eu) at the exact position of the target. The obtained absolute efficiency is displayed in Fig. 2.13.

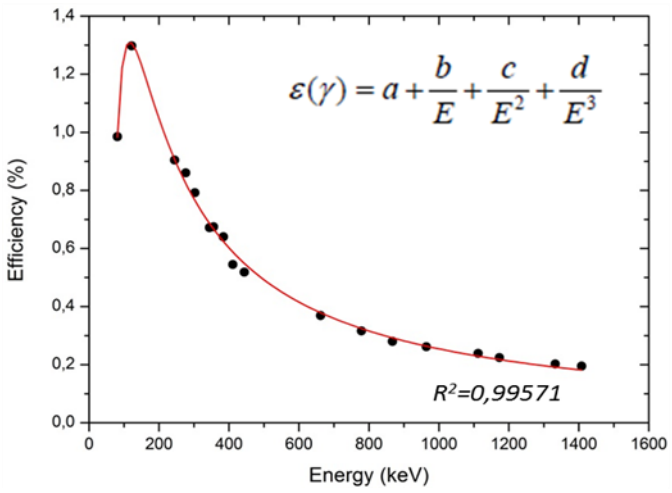

Fig. 2.13. Absolute detector efficiency of the HPGe detector.

All measurements have been completed and analysis of the data is in progress. A typical γ-ray spectrum from the Al target measured with 2.860 MeV protons is shown in Fig. 2.14.

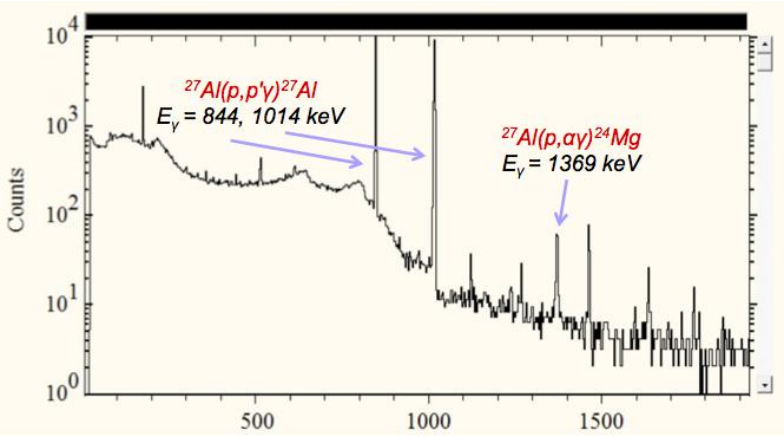

Fig. 2.14. γ-ray spectrum from Al target measured with 2.860 MeV protons.

Parallel to the cross section measurements, the PIGE method was applied for quantification of beryllium in mineral Euclase – $BeAl[SiO_4]OH$ using reaction $^{9}Be(p, \gamma)^{10}B$, E_γ=718 keV at E_p = 1.2 MeV. The beam spot on the target was 3 mm. As a reference material pure Be foil was used. Several spots of crystal (Euclase Mina) were analysed and the results obtained differ from 4.67 to 7.33 % wt. Crystals from different location (Euclase Jacu) were also analysed with the TOF-ERDA method and a concentration of 6.68 % wt. was measured.
Quantification of fluorine and sodium in dental alloys was performed using reactions: $^{19}F(p,p'\gamma)^{19}F$, Eγ = 110 and 197 keV, $^{23}Na(p,p'\gamma)^{23}Na$, E_γ = 440 keV at 2.4 MeV proton energy. As a reference material LiF and NaCl were used. Measurements were performed both, in vacuum and in the air.

2.8. Differential cross section measurements of the $^{32}S(p,p'\gamma)^{32}S$ reaction, A. Lagoyannis

During the first year of the CRP, the following actions were performed according to the submitted proposal and the suggestions made at the first Research Coordination Meeting:

1) Extensive literature research for $^{32}S(p,p'\gamma)^{32}S$ measurements performed in the past.
2) Measurement of the 991 keV $^{27}Al(p,\gamma)$ resonance using standard aluminum target.
3) Measurement of the $^{32}S(p,p'\gamma)^{32}S$ excitation function in the energy range between 3 – 6 MeV.

2.8.1. Data from previous $^{32}S(p,p'\gamma)^{32}S$ measurements

An extensive literature search revealed that in previous works on the subject four resonances appear in the region between 3 and 4 MeV, two of which are especially strong and thus suitable for in-depth analysis. On the other hand, the authors disagree not only on the exact energy of the excitations but also on the magnitude of the cross sections. In Table 2.4 these results are summarized including the expected position of the resonances according to the levels reported in Nuclear Data Sheets.

Table 2.4. Data on the $^{32}S(p, p'\gamma)^{32}S$ reaction as found in literature

	Resonance energy (keV)			**Cross Section at 90^o (mb×keV/sr)**			**Cross Section at 0^o (mb×keV/sr)**		
	1st res.	2nd res.	3rd res.	1st res.	2nd res.	3rd res.	1st res.	2nd res.	3rd res.
Ref. [2.10]	3089	3379	3717	8	30	35	18	64	70
Ref. [2.11]	3095	3379	3716	10.88	41.84	48.10	-	-	-
Ref. [2.12]	3094	3379	3716	-	-	-	-	-	-
Ref. [2.13]	3094	3376	3715	-	-	-	-	-	-

As can be seen from Table 2.4, a new measurement including more angles is required in order to provide the PIGE community with reliable data.

2.8.2. Measurement of the 991 keV resonance of the $^{27}Al(p,\gamma)$ reaction

A measurement of the well-known resonance of the $^{27}Al(p,\gamma)$ reaction at the proton energy of 991 keV using a HPGe detector of 50% relative efficiency placed at 90^o was performed using a standard thick aluminum target. The results of this measurement are presented in Fig 2.15.

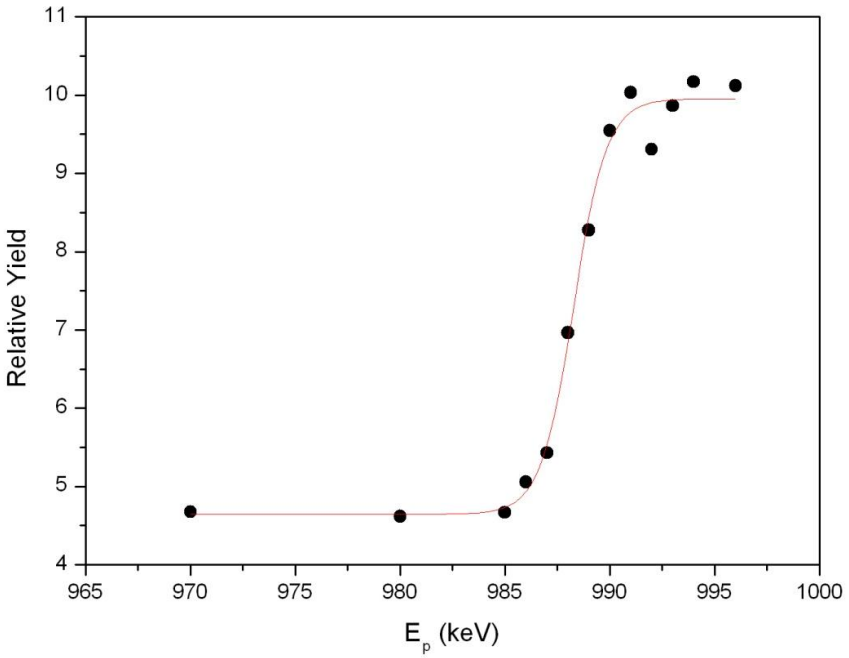

Fig. 2.15. Excitation function of the $^{27}Al(p,\gamma)^{28}Si$ reaction at 90^o.
The red curve is the fit of data with a step function.

2.8.3. Measurement of the $^{32}S(p,p'\gamma)^{32}S$ excitation function in the energy range of 3 to 6 MeV

As mentioned above, the availability of data for the $^{32}S(p,p'\gamma)^{32}S$ reaction is limited in energy range and number of measured angles. Moreover, the reported yields exhibit differences that render the use of this data questionable. In the framework of the present CRP, a measurement of the $^{32}S(p,p'\gamma)^{32}S$ reaction was made in a wider energy and angular range, aiming at resolving

these ambiguities.
The first challenge in such an experiment is the production of a thin, thermal, robust target with known stoichiometry. For the production of the target, various methods (e-gun sputtering and thermal evaporation) were used in combination with different sulfur compounds (CdS and FeS), but unfortunately all of them resulted in thermal sensitive targets with unknown stoichiometry as was proven by RBS measurements. The solution that finally rendered the expected results was the one proposed by J.P. Greene and C.J. Lister [2.14]. According to this method, MoS_2 is diluted into isopropanol and then sprayed with an airbrush onto thin carbon foils. Following this method, targets of various thicknesses were produced and then characterized using the RBS method before and after the experiment.
The measurement of the excitation function was made in the energy range between 3 and 6 MeV, with a varying step of 2 to 20 keV, depending on the proximity to resonances. The beam current was kept at 100 nA throughout the whole measurement and was constantly monitored by a thick (1000 μm) SSB detector, which was mounted at an angle of 140^o with respect to the beam. The 2230 keV gamma ray yield from the de-excitation of ^{32}S was detected by three HPGe detectors placed at 0^o, 55^o and 125^o degrees. The choice of 55^o and 125^o (-55^o) was made in order to check whether the angular distribution of the 2230 keV gamma ray is isotropic or not. Moreover, for the first four resonances, which are more suitable for resonant PIGE analysis, yields for three additional angles were taken (15^o, 90^o and 155^o). The reason for these additional measurements is that, as shown by J. W. Olness *et al.* [2.12], the resonances at these energies are expected to have a rather prominent angular distribution. The distance between the detectors and the target was chosen to be between 20 and 30 cm in order to keep the angular uncertainty less than 7^o degrees for each detector.
The efficiency calibration of the detection system was done by using two calibrated gamma ray sources: ^{152}Eu for the low lying gamma rays and ^{226}Ra which gives gamma rays at the vicinity of sulfur's 2230 keV peak. In Fig. 2.16, the on-line analysis of data for the excitation function of the detector at 55^o is presented.

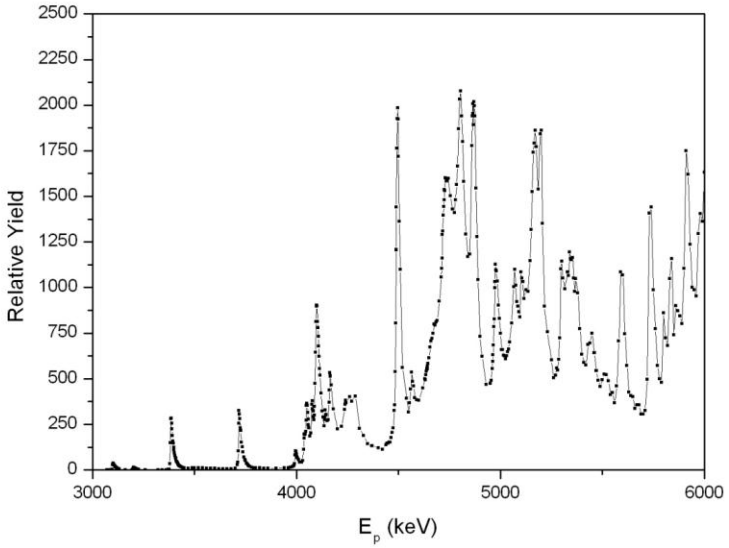

Fig. 2.16. Excitation function of the $^{32}S(p,p'\gamma)^{32}S$ reaction at 55^o.

As can be seen in Fig. 2.16, the energy region above 4 MeV is dominated by strong overlapping resonances and is therefore not suitable for PIGE analysis. For this reason, the analysis was focused in the energy region between 3 and 4 MeV. In Fig. 2.17 the cross sections for the three

measured angles (0^o, 55^o, 125^o) are compared.

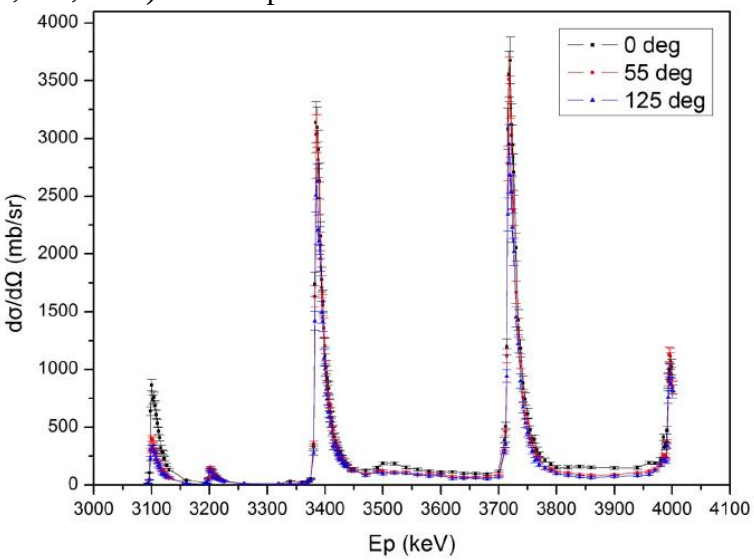

Fig. 2.17. Cross sections of the $^{32}S(p,p'\gamma)^{32}S$ reaction at 0^o, 55^o and 125^o.

From the comparison it is obvious that the cross section at 0^o is higher, especially on the resonances, indicating the existence of a strong angular dependence. Further analysis, taking into account data from three additional angles, revealed that there is indeed a non-isotropic angular distribution. The results of the present work are in very good agreement with the early work of Olness *et al.* [2.12] (Fig. 2.18).

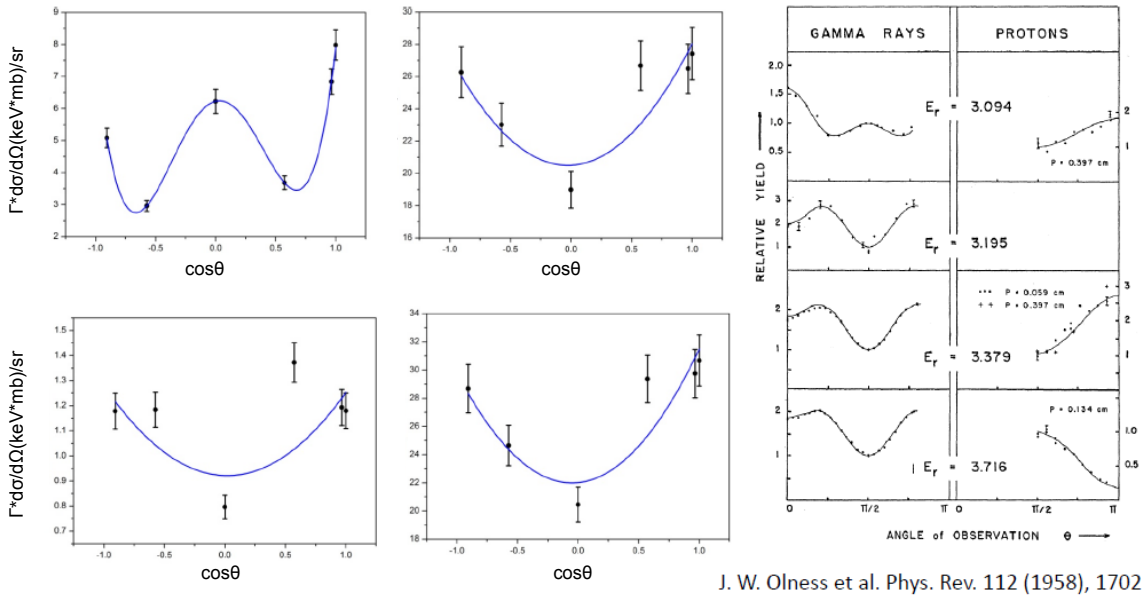

Fig. 2.18. Angular distributions of the four resonances in the 3 – 4 MeV energy region.

Finally, a comparison between the on-resonance cross section obtained in the present work and the ones already existing in the literature was made (Table 2.5). The significantly lower values of the present work can be possibly attributed to the strong angular dependence of the resonances which was not taken into account in previous works (the angular uncertainty in the previous

experiments was between ± 20^o – 30^o while in the present one was only ± 10^o).

Table 2.5. Comparison of on-resonance cross sections.

	Cross Section at 90^o (mb×keV/sr)			Cross Section at 0^o (mb×keV/sr)		
	1^{st} res.	2^{nd} res.	3^{rd} res.	1^{st} res.	2^{nd} res.	3^{rd} res.
Rao, et al. [2.10]	8	30	35	18 ± 1	64 ± 3	70 ± 6
Tsartsarakos, et al. [2.11]	10.88	41.84	48.10	-	-	-
Present Work	6.2 ± 0.4	19.0 ± 1.1	20.5 ± 1.2	8.0 ± 0.5	27.5 ± 1.6	30.7 ± 1.8

2.9. PIGE measurements at IPNAS, D. Strivay, et al.

The nuclear physics installations at the Institut de Physique Nucleaire Atomique et de Spectroscopie, Liege, include three accelerators, a 2 MV Van de Graff covering energies from 0.5-2 MeV, a 2.5 MV Van de Graff accelerator covering energies from 0.5-2.5 MeV and 0.5-4.5 MeV, and a variable energy Cyclotron covering energy ranges from 2.7-23 MeV, 4-20 MeV and 5.5 -22 MeV. These installations offer a wide and unusual variety of ion/energy conjunctions and irradiation possibilities at IPNAS, thus allowing for a wide range of activities in Applied Physics, including materials sciences using Ion Beam Analysis techniques, as well as in Fundamental Physics with contributions to fundamental experimental databases through measurements of spectroscopic levels and radiative life-times, high-energy X-ray production rates and non-Rutherford cross sections in the 6-20 MeV energy region among others.

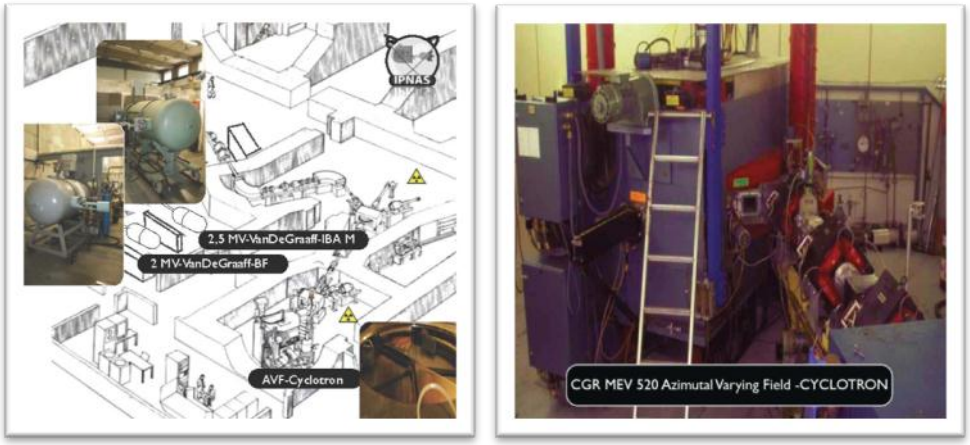

Fig. 2.19. Overview of the experimental hall with the three accelerators and a close-up view of the AVF-Cyclotron at IPNAS.

The IPNAS plans to contribute to the PIGE CRP by performing measurements at the high energy part of the relevant energy spectrum. With the cyclotron it will be possible to produce proton beams at energies ranging from 3 – 10 MeV with a good resolution. However, the energy calibration is not as straightforward as in the case of linear accelerators. The main reason being that the method of energy calibration used at large, is based on energy scanning of narrow resonances of a nuclear reaction. However, to scan the entire energy window of a few MeVs with a cyclotron, one has to vary the cyclotron magnetic parameters and optic parameters at every energy step. As these variations of cyclotron parameters are rather strong, linearity between the various energy steps is lost and hence interpolations or extrapolations in energy are not

applicable.
An alternative method of energy calibration that would allow for an absolute, direct and systematic readout of the mean energy of the primary beam, is proposed. The method is based on the measurement of the time of flight of a bunch of particles to travel a fixed distance. Using appropriate conversion techniques the measured Time-of-Flight is converted to energy.

The adaptation of the experimental setup for the implementation of the TOF method, was performed by a step-by-step approach. At each step, a specific question/problem relating to the typical timings that should be measured, the detectors that should be used to provide start and stop signals, how to distinguish events when applying the method to a beam of particles, has been addressed and solutions have been proposed.

The final optimal setup has been agreed upon, and the mounting of the new system is foreseen to be concluded in the forthcoming month. This independent start/stop set-up configuration will allow displacement of the system to other beam lines, set ups, and applications.

Finally, PIGE cross sections will be measured in the energy range from 3 to 10 MeV. The targets will be produced by the Space center of ULg.

2.10. Preliminary data for the $^{27}Al(p,p'\gamma_1)^{27}Al$, $^{27}Al(p,p'\gamma_2)^{27}Al$ and $^{27}Al(p,p'\ \gamma_{2\text{-}1})^{27}Al$ reactions at CMAM-UAM, A. Zucchiatti, et al.

2.10.1. Accelerator Calibration

For low energies we used *a)* the two resonances of the nuclear reaction $^{27}Al(p,\gamma)^{28}Si$ at 991.7 and 1316.8 keV on thick commercial (Goodfellow) target, and for high energies, as recommended during the 1st RCM *b)* RBS from MnSnO and the reaction $^{11}B(p,\alpha)^{8}Be$ on thin samples. For case *a)* the real terminal voltage has been computed from the equation $TV_{real} = \frac{1}{2}(E_{res} - V_{ext} + E_{lost})$

while in case *b)* it has been deduced from a system of 3 kinematical equations that are solved for the beam energy E_0 and then provide $E_0 = V_{ext} + 2TV_{real}$.
The combination of the two data sets gives a calibration curve that associates the real to the nominal terminal voltage.

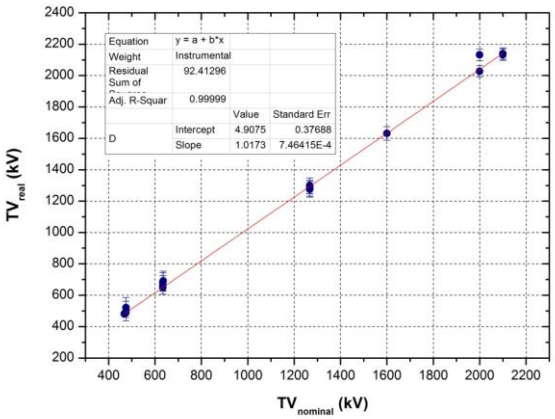

Fig. 2.20. Accelerator calibration curve.

2.10.2. The Scattering Chamber

Installed together with the accelerator in 2002 by HVEE, the Standard Beamline at CMAM is a multipurpose line, mainly used for "classical" IBA techniques as well as Ion-Beam Modification of Materieals (IBMM) over small areas. It has a 420 mm diameter experimental chamber, equipped with a 4 axis goniometer. A Reverse Electrode Coaxial Ge (ReGe) at 135 degrees with respect to the beam direction and a LaBr3 detector at 45 degree are used temporarily for gamma ray spectroscopy. Two implanted silicon detectors (one fixed and one movable) are used for charged particle detection. Only the fixed detector has been used in the PIGE cross-section measurements.

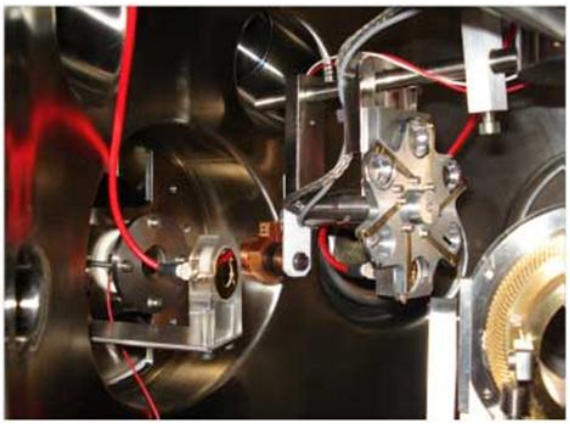

Fig. 2.21. Experimental setup for charged-particle detection.

2.10.3. Gamma-ray Detectors Efficiency

The absolute efficiency of both the ReGe and Lanthanum Bromide ($LaBr_3$) gamma detectors has been measured using calibrated sources in two different set-ups. In our "ToF chamber" we used ^{133}Ba and ^{22}Na sources (5%). Then the measured absolute efficiencies *Eabs* have been fitted with a power function and rescaled (by the squared ratio of target detector distances) to the "Standard chamber" geometry, where cross sections have been measured. In a second step the ReGe and $LaBr_3$ detector efficiency has been calibrated with ^{137}Cs and ^{60}Co sources (1%). The graph for the ReGe detector takes into account also preliminary Montecarlo calculations, while the $LaBr_3$ graph is limited to the data obtained with sources.

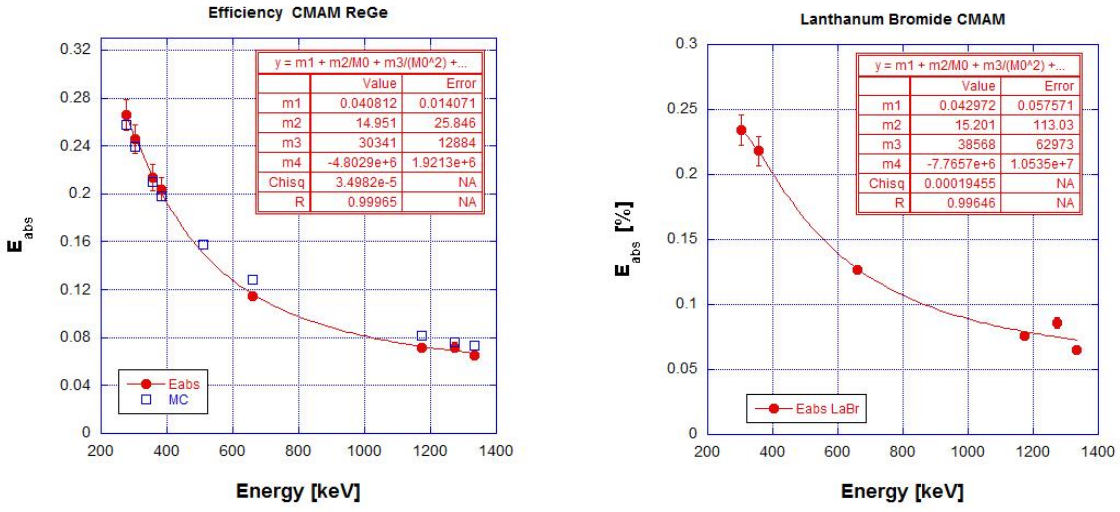

Fig. 2.22. Absolute efficiency of Gamma-ray detectors.

2.10.4. Target Preparation

The samples were prepared with the magnetron sputtering technique. A calibration of the sputtering system at CMAM was performed in order to control the thickness of the Al and Ag layers. For the sputtering calibration six different samples were prepared: three samples with Ag and three with Al. Each sample was prepared with a different sputtering time, the thicknesses of the different Ag and Al layers were determined with the RBS technique. The simulations of the layers were performed with the program RBX.

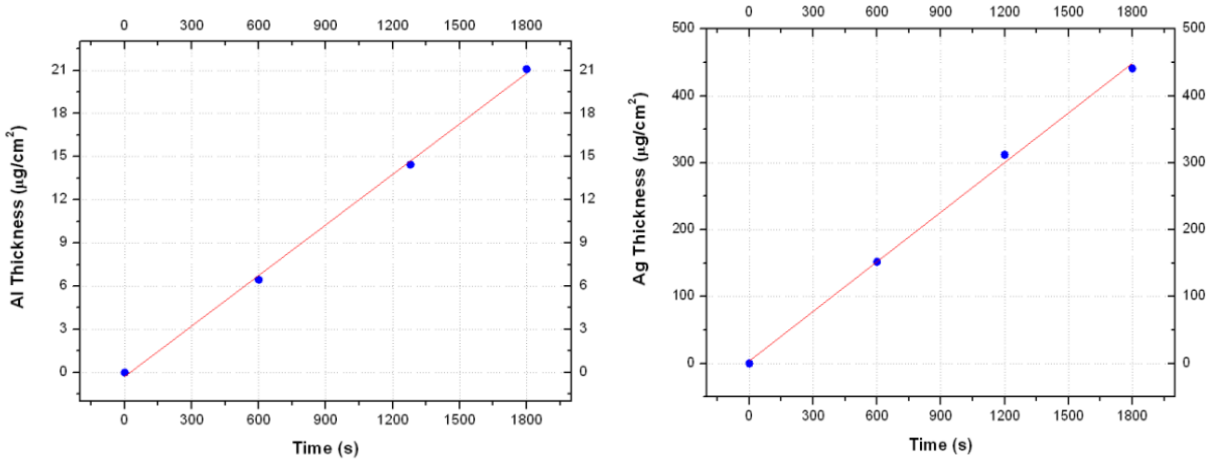

Fig. 2.23. Calibration of sputtering system using samples with Ag and Al.

With this calibration we calculated the sputtering time necessary for the nominal thicknesses required for this experiment: 15 μg/cm^2 of Al over 45 μg/cm^2 of Ag; the substrate was a carbon foil of 56 μg/cm^2. A double check is ongoing on the Al and Au thickness using alpha particle RBS: therefore our cross-section values are not to be taken as absolute values yet.

2.10.5. Cross-Section Measurements on Al

We scanned the energy range from 2500 keV to 3200 keV in 10 keV steps. As part of the IAEA CRP program we have measured the ^{27}Al(p,p´γ_1)^{27}Al (E_γ = 844 keV), the ^{27}Al(p,p´γ_2)^{27}Al (E_γ = 1014 keV) and the ^{27}Al(p,p´$\gamma_{2\text{-}1}$)^{27}Al (E_γ = 171 keV); the 171 keV peak is isolated on a well subtractable background. The need to measure the target thickness precisely and re-check the MC efficiency calculations for the moment prevents the assignment of an absolute cross-section value. The analysis of further peaks like ^{27}Al(p,αγ)^{24}Mg (E_γ = 1369 keV) and ^{27}Al(p,γ)^{28}Si (E_γ = 1779 keV) is difficult because their peak shape is not gaussian and the peak-to-background ratio is high. Higher energy peaks do not produce, at the energies scanned, statistically significant yields. In the first part of the experiment it became evident that the collimation slits just before the STD chamber were producing a variable aluminium gamma background, most probably generated in the aluminium parts that hold the tantalum slits and depending on the beam fine alignment. This has been cured by positioning a tantalum foil with a 2 mm diameter hole in front of the slits. The measurements taken in the above conditions were then repeated. A careful analysis needs to be done to subtract the slits background before the data is eventually used for cross-section calculations. Due to the superior resolution of the germanium spectrometer, and the decreasing detector efficiency of the $LaBr_3$ detector , because of the FC shielding of this detector and not calculated, and also due to the fact that the LaBr3 detector was positioned at an angle (45º) that does not correspond to those selected by the CRP (135, 90, 55),

we present for the moment the REGe data only. The yield curves on the ReGe and $LaBr_3$ detector are indeed quite similar.

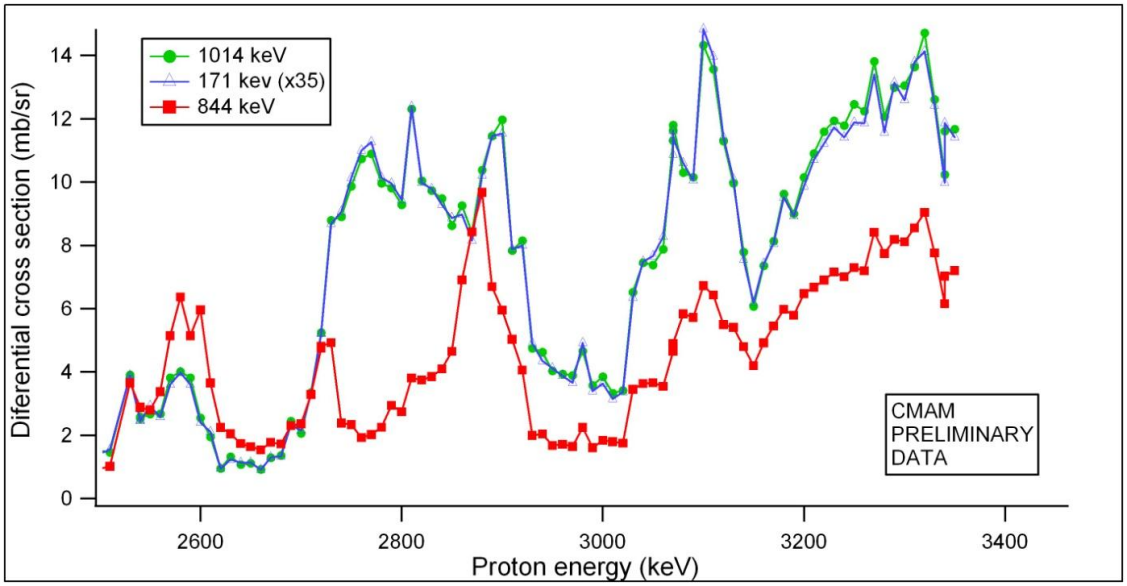

Fig. 2.24. Cross sections of the $^{27}Al(p, p'\gamma)^{27}Al$ reaction.

The statistical errors on the three peaks are much lower than the error on the detector absolute efficiency (we estimate 2% maximum), the error on the target thickness (we cannot discard so far a systematic error linked to the sputtering calibration) and the possible systematic error on the collected charge. The conversion of Ag backscattered proton counts into charge through the Rutherford cross section for normalization was not used. At the same energy and point RBS spectra are always reproducible: the silver peak very closely follows a Rutherford behavior with a maximum of a 4% deviation from a $1/E^2$ energy dependence, proving that the collected charge is stable. The Al peak follows closely the published data of Chiari et al. [2.15].

2.11. Measurement of excitation yields of low energy prompt γ-ray from proton bombardment of Ti-foils with energies ranging between 1.0 and 3.0 MeV, A.V. Goncharov, et al.

The aim of this work is the measurement of differential cross sections for the production of the 90.6 keV γ-ray from the reactions $^{48}Ti(p,\gamma)^{49}V$ and $^{48}Ti(p,\gamma)^{49}V+^{49}Ti(p,n\gamma)^{49}V$ for proton energies ranging between 1.0 and 3.0 MeV at the laboratory angle of 90^0 using targets of 3.7×10^{18} at/cm^2 for ^{48}Ti and 1.86×10^{18} at/cm^2 for ^{nat}Ti. For this purpose the following activities were carried out.

A new beam line for measurements of low energy prompt γ-ray emission was constructed at ESU-5 accelerator. The energy calibration of the accelerators "Sokol" and ESU-5 was performed using the resonances in the $^{27}Al(p,\gamma)^{28}Si$ reaction.

TiN targets (natural Ti) on carbon backings were prepared by the ion beam assisted deposition (IBAD) technique. The thickness (at/cm^2) and stoichiometry of the targets were measured by using back-scattering spectrometry with He and H ions at energies ranging between 1.6 and 1.8 MeV.

The measurement of low-energy γ-rays was performed by means of a thin HPGe-detector. Calibration of the γ-ray detector efficiency was carried out with the standard ^{133}Ba, ^{152}Eu, and ^{241}Am sources with the same geometry used for the cross-section measurements.

The excitation functions for the production of 90.6 keV γ-rays from reactions $^{48}Ti(p,\gamma)^{49}V$ and

^{48}Ti(p,γ)^{49}V+^{49}Ti(p,nγ)^{49}V for proton energies ranging between 1.0 and 3.0 MeV at the laboratory angle of 90^0 have been measured. The experimental data have been analysed and tabulated.

The typical spectrum of low-energy γ-rays from the ^{48}Ti/Ta target are presented in Fig. 2.25.

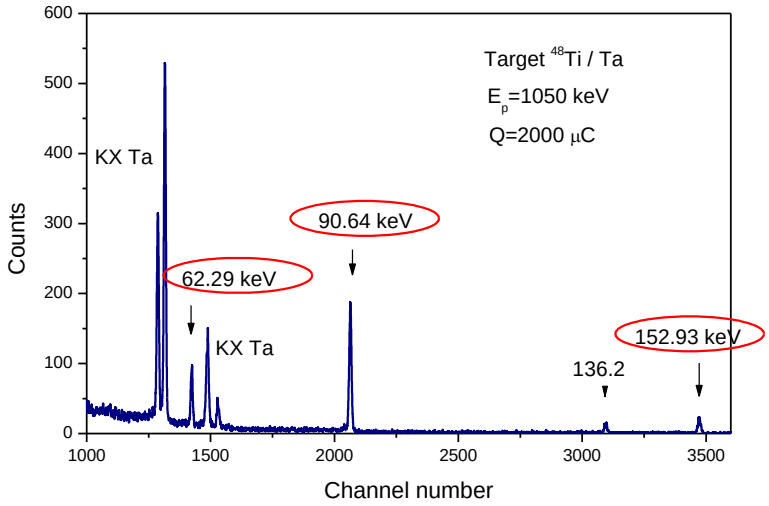

Fig. 2.25. The typical spectrum of low-energy γ-rays from the ^{48}Ti target on Ta backing.

The typical spectrum of low-energy γ-rays from the ^{nat}TiN/C target are presented in Fig. 2.26

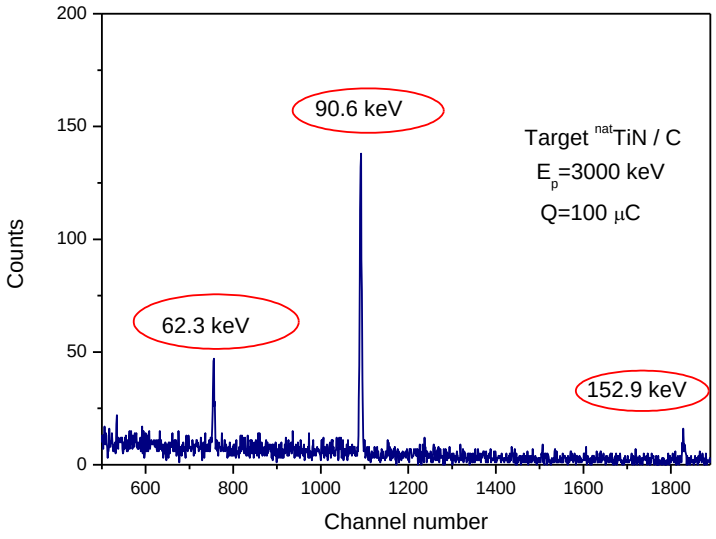

Fig. 2.26. The typical spectrum of low-energy γ-rays from the ^{nat}TiN target on C backing.

The averaged differential cross-section $d\sigma/d\Omega$ of γ-ray production from the ^{48}Ti(p,γ)^{49}V reaction was determined from the general expression:

$$d\sigma/d\Omega = N_\gamma \cos\varphi / 4\pi\, \varepsilon\, k\, N_p\, f\, t$$

where
N_γ is the number of counts in the full-energy peak,
k is the ratio between the live time and the exposure time,
N_p is the number of protons incident upon the target,
$\varepsilon = \varepsilon(E_\gamma)$ is the efficiency of the detection system,
f is the relative content of ^{48}Ti in Ti target substance,
t is the Ti target thickness (at/cm^2),
Φ is the beam incidence angle taking from normal to the target.

The results of the measured differential cross-sections for the production of 90.6 keV γ-ray from the reactions ^{48}Ti(p,γ)^{49}V and ^{48}Ti(p,γ)^{49}V+^{49}Ti(p,nγ)^{49}V, $\theta_{lab}=90^0$ are presented in Fig. 2.27.

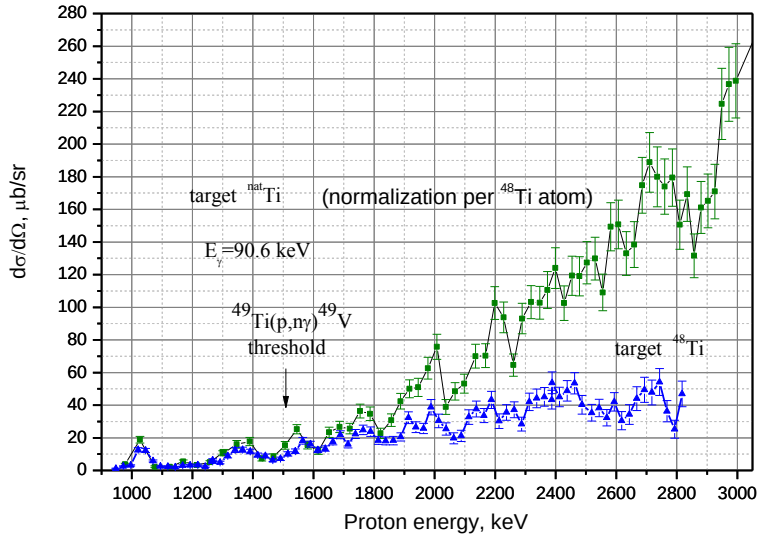

Fig. 2.27. Comparison of the excitation function for the production of 90.6 keV γ-rays from reactions ^{48}Ti(p,γ)^{49}V and ^{48}Ti(p,γ)^{49}V+^{49}Ti(p,nγ)^{49}V on ^{nat}Ti-target with the excitation function for the production of the 90.6 keV γ-ray from the reaction^{48}Ti(p,γ)^{49}V on ^{48}Ti-target for proton energies ranging between 900 and 3000 keV at the laboratory angle of 90^0.

2.12. Modification of IBANDL to accommodate PIGE data- Study of the feasibility of producing evaluations for PIGE A. Gurbich.

According to the plan for special actions accepted at the 1st RCM the necessary changes were made in IBANDL and in the R33-format to accommodate PIGE data. The data to be included in IBANDL are differential cross sections and thick target yields. IBANDL was modified in order to enable it to deal with both kinds of data.
The following change was made in the R33 format: for PIGE data an additional entry "Egamma:" which contains the gamma-ray energy in keV was inserted, the sign '+' being used between the energies for unresolved lines. This entry is used as a flag to identify PIGE data and to sort files in the table of the retrieved data according to the γ-ray energy. The γ-ray energy is

also displayed in the table of retrieved data. A corresponding change was also made in the template used for the upload of the R33 files. The lines with PIGE data are placed at the bottom of the table after EBS and NRA data. A new unit "yield" was introduced in the R33 format. The data presented in this unit should contain a thick target yield of gammas in N_γ / sr μC.
The script producing IBANDL graphics was modified to plot the data in the "yield" units. However, the possibility to compare the data presented in R33 files as cross-sections and yield in the same plot has not been implemented yet because of the lack of a light version of ERYA code which could be called by IBANDL to perform calculations of target yields using the differential cross section data.
The work on transferring EXFOR files relevant to PIGE into IBANDL was hampered by the interruption of the remote access to the server due to computer security measures introduced in the IAEA.
The feasibility of producing evaluations for PIGE was studied according to the plan of special actions. The gamma emission used in PIGE is of two kinds – primary γ-rays and cascade ones. For primary gammas the excitation function can be calculated using the R-matrix theory and a good agreement between theory and experiment can be achieved as was demonstrated for the $^{12}C(p,\gamma)^{13}N$ reaction [2.16]. As for cascade gammas emitted by light nuclei, it is not clear how to theoretically reproduce resonances in the reaction entrance channel. For nuclei of medium weight and heavy nuclei for which the excitation function is usually smooth, it is possible to calculate cross-sections and angular distributions of gammas in the framework of the statistical model. The corresponding formulas are presented in [2.17]. An example of the evaluation of the angular distribution for gammas from $^{56}Fe(n,n'\gamma)^{56}Fe$ reaction is given in [2.18]. It should be noted that the evaluation implies the availability of at least more than one data set. As the evaluation starts with data compilation, an attempt to evaluate the angular distribution for the case relevant to PIGE can be made provided suitable data are measured or found in the literature. Generally further work on the elaboration of an approach to theoretical calculations of the PIGE differential cross-sections is needed and it is highly desirable that a professional theoretician is involved in the work.

References

[2.1] Lisbon Group, present work (to be published).

[2.2] R. Mateus, A.P. Jesus, J. Cruz, J.P. Ribeiro, Measurement of the inelastic scattering of protons by 23Na in the energy range 1.25–2.40 MeV, Nucl. Instr. and Meth. B **219-220** (2004) 3.7-311.

[2.3] A. Caciolli, G. Calzolai, M. Chiari, et al., Proton elastic scattering and proton induced γ-ray emission cross-sections on Na from 2 to 5 MeV, Nucl. Instr. and Meth. B **266** (2008) 1392-1396.

[2.4] H. van Bebber, L. Borucki, K. Farzin, Á.Z. Kiss, W.H. Schulte, Total cross section of the $^{14}N(d,p\gamma)^{15}N$ nuclear reaction for analytical applications, Nucl. Inst. Methods B **136–138** (1998) 72-76.

[2.5] O.R. Kakuee, V. Fathollahi, P. Oliaiy, M. Lamehi-Rachti, R. Taheri, H.A. Jafarian, External PIXE analysis of an Iranian 15th century poetry book, Nucl. Instr. and Meth. B **273** (2012) 178-181.

[2.6] O.R. Kakuee, V. Fathollahi, M. Lamehi Rachti, Ion beam analysis of hydrogen in advanced materials: Recent experience of Van de Graaff lab, Int. J. Hydrogen Energy **35** (2010) 9510-9515.

[2.7] M. Goudarzi , *et al.*, L-sub shell and total M-shell X-ray production cross sections of Ta, W, Pt, Au, Pb and Bi by 0.7-2.4 MeV protons, Nucl. Instr. and Meth. B **247** (2006) 217-222.
[2.8] A. Amirabadi, *et al.*, L subshell and total M shell x-ray production cross sections of Hg for protons of energy 0.7-2.9 MeV, J. Phys. B: At. Mol. Opt. Phys. **30** (1997) 863-872.
[2.9] F. Shokouhi, *et al.*, M-Shell X-ray production Cross sections of Tb, Ho, Tm and Lu for protons of Energy 2-6 MeV, Nucl. Instr. and Meth. B **109** (1996) 15-18.
[2.10] Pritty Rao, Sanjiv Kumar, S. Vikramkumar, V.S. Raju, Measurement of differential cross-sections and widths of resonances in $^{32}S(p,p'\gamma)^{32}S$ reaction in the 3.0–4.0 MeV region, Nucl. Inst. Meth. B **269** (2011) 2557.
[2.11] C. Tsartsarakos, P. Misaelides, A. Katsanos, Cross sections for the $^{32}S(p, p'\gamma)^{32}S$ nuclear reaction used for the profiling of sulphur on materials surfaces, Nucl. Inst. Meth. B **45** (1990) 33.
[2.12] J. W. Olness, W. Haeberli, H.W. Lewis, Levels of ^{33}Cl from $^{32}S(p, p)^{32}S$ and $^{32}S(p,p'\gamma)^{32}S$ Phys. Rev. **112** (1958) 1702.
[2.13] J. Chen, B. Singh, Nucl. Data Sheets **112** (2011) 1393.
[2.14] J.P. Greene, C.J. Lister, The production of sulfur targets for γ-ray spectroscopy, Nucl. Inst. Meth. A **480** (2002), 79.
[2.15] M. Chiari, L. Giuntini, P.A. Mandò, N. Taccetti, Proton elastic scattering cross-section on aluminium from 0.8 to 3 MeV, Nucl. Instr. Meth. B174 (2001) 259.
[2.16] R.E. Azuma, E. Uberseder, E. C. Simpson,et al. AZURE: An R-matrix code for nuclear astrophysics, Phys. Rev. C **81** (2010) 045805.
[2.17] E. Sheldon, D.M. Van Patter, Compound inelastic nucleon and gamma-ray angular distribution for even-and-odd-mass nuclei, Rev. Mod. Phys. **38** (1966) 143.
[2.18] M.V. Savin, A.V. Livke, A.G. Zvenigorodskiy, The evaluation of angular distribution and cross-sections for the formation of discrete gamma-lines of iron, Voprosy Atomnoy Nauki i Techniki. Ser.: Yadernie Konstanti, 1999, #2, p. 77.

3. Methodology

CRP participants have carried out measurements as discussed in the first RCM and presented in Table 4.1. The analysis of the existing literature is in progress and some data have already been submitted to IBANDL. This activity along with pending measurements will continue until the third RCM in spring 2014. In parallel, the assessment of the newly measured data will be carried out by the participants according to the assignments indicated in Table 4.3. Some specific aspects regarding the methodology that were revisited in this meeting are presented in the following sections. It was already agreed upon in the first RCM, that to identify possible sources of discrepancies and systematic errors among the different laboratories participating in the measurements, inter-laboratory comparison measurements were absolutely necessary. Such measurements have already started and will be completed before the end of February 2013. The importance of thick target benchmark experiments was again emphasized. A working version of the ERYA code was presented and will be used for processing data. The participants also agreed that, in the long run, a program with the capability to analyze depth profiles should be developed. A beta version of such a program is described in the following section.

3.1. Codes for PIGE

As was already pointed out in the first RCM, the aim of standard less PIGE could be achieved if, apart from the differential cross sections compiled in the reference database, the community is also provided with a reliable computer code for use of the database and calculation of the quantities needed by the user.

The ERYA code was demonstrated and was shown to be capable of calculating simultaneously the mass concentration of an arbitrary number of elements in a homogeneous sample (any thickness). Furthermore, it has the capability of fitting the sample matrix composition. For details see http://www-nds.iaea.org/pige/index2.html (ERYA presentation by A. Pedro de Jesus). Future developments include the option of using IBANDL cross-section data directly in the R33 format and dealing with in-depth heterogeneous samples.

Another code was demonstrated by A. Gurbich which uses Tichonov's regularization method [3.1] to resolve the ill-posed problem of deriving a depth profile from experimental data in the case where the excitation function has more than one resonance in the effective energy region.

3.2. PIGE data in IBANDL database

The R33 format has been modified to include additional information specific to PIGE. Data submitted to IBANDL are still not available due to new IT security measures implemented in the IAEA. Some special options in IBANDL, such as uploading data in the R33 format and the automatic transfer of data from EXFOR, are still not working but they are expected to become available soon. The data to be included in IBANDL are differential cross sections and thick and intermediate target yields. Information about angular distributions and resonance strengths will be included in the Comment section of the corresponding R33 file. IBANDL should also be supplied with an option to visually compare differential cross-section data and thick-target yields on the fly.

3.3. Energy calibration of accelerators

Preliminary data presented at this meeting show deviations of ±5 keV between the different values of accelerator energies at ~3MeV and it was agreed that it was imperative to reduce the deviation to below ±2 keV. The approach to harmonize the calibration procedure at different laboratories was discussed and accepted. Some experimental results and methods of energy calibration were shown in the presentations (see http://www-nds.iaea.org/pige/index2.html)

3.4. Target preparation

Target preparation was discussed and the methodology to prepare Al_2O_3 thin films was explained by A. Gurbich. As in the previous RCM, there was an agreement to share targets among the participants. Concerning targets the following comments were made, in particular:

- for Na, NaCl was suggested again deposited on a Ag film;
- for thin Silicon nitride targets, it was mentioned that properties given by the manufacturer were not reliable and should be checked by IBA methods;
- thick boron targets could be produced by pressing boron powder or using commercial boron nitride samples;
- concerning good-quality targets provided by commercial companies one could obtain targets with a thickness of ~20μg/cm^2 deposited on polymeric substrate.

3.5. Absolute cross-sections measurements

The total cross section may be derived from the following expression assuming isotropy

$$\sigma_\gamma(E_0) = \frac{Y_\gamma(E_0)}{N_p N_T \varepsilon_{abs}(E_\gamma)}, \qquad (1)$$

where $Y_\gamma(E_0)$ is the measured γ-ray yield (i.e. the area of the γ-ray peak) at projectile energy E_0, N_p is the number of incident projectiles, N_T is the number of target nuclei per square centimetre and $\varepsilon_{abs}(E_\gamma)$ is the absolute efficiency of the γ-ray detector corresponding to the E_γ energy γ-ray line. However, if there is anisotropy in the angular distributions, a correction factor depending on the detector angle θ and the detector aperture must be applied. A way to deal with anisotropy would be to place the detector at an angle θ = 55° or 125°.

Due to the fact that for a gamma-ray detector the split between intrinsic efficiency and solid angle is not well defined, and therefore only the absolute efficiency may be calculated and measured, it was discussed whether this would affect angle-differential cross-section measurements.

Taking into account that the 4π gamma-ray yield, Y^{em}, may be written as

$Y^{em} = \sigma_\gamma N_p N_T$,

where N_p and N_T are the number of incident projectiles and number of atoms per surface unit, respectively, and σ_γ is the total cross section. This may be written in terms of the angular differential cross section $d\sigma/d\Omega$ as

$$Y^{em} = \left(\int \frac{d\sigma}{d\Omega} d\Omega \right) N_p N_T .$$

For isotropic gamma radiation and for a detection solid angle $\Delta\Omega$ assumed to be small, we may write for the yield of gamma radiation going to the detector, Y^{gd}, that

$$Y^{gd} \approx \frac{\Delta\sigma}{\Delta\Omega} N_p N_T \, \Delta\Omega \qquad \text{or} \qquad Y^{gd} \approx 4\pi \times \frac{\Delta\sigma}{\Delta\Omega} N_p N_T \frac{\Delta\Omega}{4\pi}$$

From the gamma radiation reaching the detector, the yield of the fraction that is detected, Y^d, is given by

$$Y^d \approx 4\pi \times \frac{\Delta\sigma}{\Delta\Omega} N_p N_T \, \varepsilon_{\text{int}} \frac{\Delta\Omega}{4\pi} \qquad \text{or} \qquad Y^d \approx 4\pi \times \frac{\Delta\sigma}{\Delta\Omega} N_p N_T \, \varepsilon_{ab},$$

where ε_{int} and ε_{ab} are the intrinsic and absolute detector efficiencies, respectively, according to the usual definition (see for example Knoll [3.2]).

Hence we arrive at the following relation

$$\frac{\Delta\sigma}{\Delta\Omega} \approx \frac{Y^d}{4\pi N_p N_T \varepsilon_{ab}}$$

which defines the angular differential cross section in terms of the absolute efficiency only and not in terms of the intrinsic efficiency or solid angle which are undefined.

3.5.1. Detector efficiency determination

The importance of the accurate determination of the absolute detector efficiency was already acknowledged at the first RCM where the recommended methodology was outlined.

In this second RCM, the methods used to determine the absolute efficiency in the experiments were discussed in detail. As relative intensity lines may vary among different databases, it was decided that one and the same database should be used by all participants. It was therefore agreed that the "Update of X Ray and Gamma Ray Decay Data Standards for Detector Calibration and Other Applications" [3.3] would be used here-to-forth, for the purposes of this CRP. It was also advised that where possible, efficiencies determined from experimental calibration points should also be checked by Monte-Carlo simulations.

Participants also agreed that a detailed account of the efficiency calibration performed in all the laboratories and how it may affect the inter-laboratory comparison of thin and thick-target measurements would be worthwhile to include in a contribution to ECAART 2013. For this purpose, a special action was added to the list of special actions (see Table 4.4)

3.5.2. Assignment of uncertainties

The participants re-iterated the importance to maintain an accurate uncertainty budget. The systematic and statistical uncertainties have to be recognized and provided in a tabular form. In the cross-section graphs only the statistical uncertainties should be plotted as uncertainty bars.

3.6. Inter-laboratory comparisons

For thin-target measurements it was decided that, in order to assess systematic problems of experimental facilities, all participants would measure the $^{27}Al(p, p'\gamma)^{27}Al$, $E\gamma$ = 844 keV (isotropic line) excitation function from 2.5 MeV to 3 MeV at 10 keV energy steps.

For thick target measurements it was suggested that participants use the target that is routinely employed in their laboratory for accelerator energy calibration. The suggested energy points were between 0.95 and 1.1 MeV with the energy step small enough to reproduce the $^{27}Al(p,\gamma)^{28}Si$ resonance at 991 keV proton energy. The gamma line of 1.779 MeV would be used. Results would be submitted for presentation at ECAART 2013.

3.7. Evaluation

An important part of the evaluation process is the theoretical calculation of differential cross section. It was agreed that computer code SAMMY (and possibly other codes) would be investigated to produce some theoretical calculations for cross sections and angular distributions relevant to PIGE.

3.8. Miscellaneous

In relation to assessment of the existing data, it was decided that those assigned to a specific nuclide (Table 4.3) would also take care of the assessment of previous published data. The references and maybe numerical data, if available, would be sent to A. Gurbich. Data in graphical format would be digitized by Valentina Semkova (EXFOR group) from IAEA/NDS.

In relation to angular distributions it was agreed to measure them only for special cases.

3.9. Dissemination of CRP results

It was agreed to submit an abstract and a paper for presentation at ECAART 2013. One of the technical aspects of that paper would be the inter-laboratorial exercise related to thin and thick Aluminium cross sections (referred above).

References

[3.1] A.N. Tichonov, Solution of incorrectly formulated problems and the regularization method, Soviet Mathematics **4** (1963) 1035-1038.

[3.2] G.F. Knoll, Radiation Detection and Measurement, 4thedition, J. Wiley and Sons, 2010.

[3.3] M.-M. Be, V.P. Chechev, V.G. Khlopin, et al., Update of X Ray and Gamma Ray Decay Data Standards for Detector Calibration and other Applications, Volume 2: Data Selection Assessment and Evaluation Procedures, IAEA Report STI/PUB/1287-VOL2, 2007.

4. Action lists

Table 4.1. Completed Measurements

Isotope	Reaction	γ-ray [keV]	Energy range [MeV]	Angle [°]	Initial State, Jπ	Type of Data	Comments	Measured by:
^{7}Li	(p,p´γ)	478	2-4	130	1/2-	Differential+ Thick target	Detailed+sparse points	Pedro de Jesus
^{9}Be	(p,γ)	718	0.5-1.7	130	1+	Differential+ Thick target	Detailed	Pedro de Jesus
^{10}B	(p,α´γ)	429	2-4	130	1/2-	Thick target	Sparse points	Pedro de Jesus
^{12}C	(p,γ)		1.1-2.6	55 and 0		Differential	Detailed	Becker
^{14}N	(p,p´γ)	2313	4-7	55	0+	Differential	Detailed+sparse points	Raisanen
^{14}N	(d,p´γ)	1885	0.6-2	55	5/2+	Differential	Detailed+sparse points	Kiss
^{14}N	(d,p´γ)	2297	0.6-2	55	7/2+	Differential	Detailed+sparse points	Kiss
^{14}N	(d,p´γ)	8310	0.6-2	55	1/2+	Differential	Detailed+sparse points	Kiss
^{19}F	(p,p´γ)	110	2-4	130	1/2-	Differential+ Thick target	Detailed	Pedro de Jesus
^{19}F	(p,p´γ)	197	2-4	130	5/2+	Differential+ Thick target	Detailed	Pedro de Jesus
^{19}F	(p,α´γ)	6000-7000	0.8-4.0	130	3-	Differential+ Thick target	Detailed	Pedro de Jesus
^{23}Na	(p,p´γ)	440	2-4	130	5/2+	Differential+ Thick target	Detailed	Pedro de Jesus
^{23}Na	(p,p´γ) (p,α´γ)	1636 1634	2-4	130	7/2+ 2+	Differential+ Thick target	Detailed	Pedro de Jesus
^{23}Na	(p,p´γ)	440	1.8-3	135	5/2+	Differential	Detailed	Bogdanovic
^{23}Na	(p,p´γ) (p,α´γ)	1636 1634	1.8-3	135	7/2+ 2+	Differential	Detailed	Bogdanovic
^{25}Mg	(p,p´γ)	390	2-4	130	3/2+	Differential+ Thick target	Detailed	Pedro de Jesus
^{25}Mg	(p,p´γ)	390	1.8-3	135	3/2+	Differential	Detailed	Bogdanovic
^{25}Mg	(p,p´γ)	585	2-4	130	1/2+	Differential+ Thick target	Detailed	Pedro de Jesus
^{25}Mg	(p,p´γ)	585	1.5-2.4	130	1/2+	Differential+ Thick target	Detailed	Pedro de Jesus
^{25}Mg	(p,p´γ)	974	1.5-2.4	130	3/2+	Differential+ Thick target	Detailed	Pedro de Jesus
^{25}Mg	(p,p´γ)	585	1.8-3	135	1/2+	Differential	Detailed	Bogdanovic
^{27}Al	(p,p´γ)	844	1.5-3	130	1/2+	Differential	Detailed	Pedro de Jesus

Isotope	Reaction	γ-ray [keV]	Energy range [MeV]	Angle [°]	Initial State, Jπ	Type of Data	Comments	Measured by:
^{27}Al	(p,p´γ)	844	2.5-5	0, 165, 55, 90	1/2+	Differential	Detailed	Lagoyannis
^{27}Al	(p,p´γ)	844	1.8-3	135	1/2+	Differential	Detailed	Bogdanovic
^{27}Al	(p,p´γ)	844	2.5-3.0	135	1/2+	Differential	Detailed	Zucchiatti
^{27}Al	(p,p´γ)	1014	1.5-4	130	3/2+	Differential	Detailed	Pedro de Jesus
^{27}Al	(p,p´γ)	1014	2.5-5	0, 165, 55, 90	3/2+	Differential	Detailed	Lagoyannis
^{27}Al	(p,p´γ)	1014	1.8-3	135	3/2+	Differential	Detailed	Bogdanovic
^{27}Al	(p,p´γ)	1014	2.5-3	135	3/2+	Differential	Detailed	Zucchiatti
^{27}Al	(p,α´γ)	1369	1.5-4	130	2+	Differential	Detailed	Pedro de Jesus
^{27}Al	(p,α´γ)	1369	18-3	135	2+	Differential	Detailed	Bogdanovic
^{27}Al	(p,α´γ)	1369	2.5-3	135	2+	Differential	Detailed	Zucchiatti
^{28}Si	(d,p γ)	1273	0.6-2	55	3/2+	Differential	Detailed	Kiss
^{28}Si	(d,p γ)	2028	0.6-2	55	5/2+	Differential	Detailed	Kiss
^{28}Si	(p,p´γ)	1779	4-7	55	2+	Differential	Detailed	Raisanen
^{29}Si	(p,p´γ)	1274	4-7	55	3/2+	Differential	Detailed	Raisanen
^{32}S	(p,p´γ)	2230	3-6	0, 15, 55, 90, 125, 155	2+	Differential	Detailed	Lagoyannis
^{48}Ti	(p,γ)	62.3/90.6	1-3	90		Differential	Detailed	Goncharov
^{nat}Ti	(p,γ)	62.3/90.6	1-3	90		Differential	Detailed	Goncharov
^{nat}Ti	(p,nγ)	62.3/90.6	1-3	90		Differential	Detailed	Goncharov

Table 4.2. Pending measurements

Isotope	Reaction	γ-ray [keV]	Energy range [MeV]	Angle	Initial State, Jπ	Type of Data	Comments	Assigned to:
^{7}Li	(p,p´γ)	478	2-3, 5-7	135	1/2-	Differential+ Thick target	Detailed + sparse points	Zucchiatti
^{7}Li	(p,n´γ)	429	2-3, 5-7	135	1/2-	Differential+ Thick target	Detailed + sparse points	Zucchiatti
^{9}Be	(α,n´γ)	4443	Limited energy	135	2+	Differential+ Thick target	Detailed + sparse points	Zucchiatti, if target is available
^{9}Be	(α,n´γ)	4443	2-10	135	2+	Differential+ Thick target	Detailed + sparse points	Strivay
^{10}B	(p,p´γ)	718	1-3	55,90	1+	Thick target	Sparse points	Kiss
^{10}B	(p,p´γ)	718	3-4	45, others	1+	Thick target	Sparse points	Chiari
^{10}B	(p,p´γ)	718	3-5	0, 55, 90,165	1+	Differential+ Thick target	Detailed+sparse points	Lagoyannis
^{10}B	(p,α´γ)	429	3-4	45, others	1/2-	Thick target	Sparse points	Chiari
^{10}B	(p,α´γ)	429	1-3	55, 90	1/2-	Thick target	Sparse points	Kiss
^{10}B	(p,α´γ)	429	1.0-3.8	0, 55, 90,165	1/2-	Thick target	Sparse points	Lagoyannis
^{11}B	(p,p´γ)	2124	3-4	45, others	½-	Thick target	Sparse points	Chiari
^{11}B	(p,p´γ)	2124	2.8-3.8	55, 90	½-	Thick target	Sparse points	Kiss
^{11}B	(p,p´γ)	2124	2.8-3.8	0, 55, 90,165	½-	Differential+ Thick target	Detailed+sparse points	Lagoyannis
^{12}C	(d,p´γ)	3089	0.6-2.0	55	½+	Differential	Detailed+sparse points	Kiss
^{14}N	(p,p´γ)	2313	3.5-4	45	0+	Thick target	Sparse points	Chiari
^{14}N	(p,p´γ)	2313	4-10	135	0+	Differential+ Thick target	Detailed+sparse points	Strivay
^{14}N	(d,p´γ)	1885	0.6-2	90	5/2+	Differential+ Thick target	Detailed+sparse points	Kakuee
^{14}N	(d,p´γ)	2297	0.6-2	90	7/2+	Differential+ Thick target	Detailed+sparse points	Kakuee
^{14}N	(d,p´γ)	8310	0.6-2	90	1/2+	Differential+ Thick target	Detailed+sparse points	Kakuee
^{19}F	(p,p´γ)	110	2-6	135	1/2-	Differential+ Thick target	Detailed	Zucchiatti
^{19}F	(p,p´γ)	197	2-6	135	5/2+	Differential+ Thick target	Detailed	Zucchiatti
^{19}F	(p,α´γ)	6000-7000	2-6	135	3-	Differential+ Thick target	Detailed	Zucchiatti
^{19}F	(p,p´γ)	110	2-10	135	1/2-	Differential+ Thick target	Detailed	Strivay
^{19}F	(p,p´γ)	197	2-10	135	5/2+	Differential+ Thick target	Detailed	Strivay
^{19}F	(p,α´γ)	6000-	2-10	135	3-	Differential+	Detailed	Strivay

Isotope	Reaction	γ-ray [keV]	Energy range [MeV]	Angle	Initial State, Jπ	Type of Data	Comments	Assigned to:
		7000				Thick target		
^{23}Na	(p,p´γ)	440	1-2.9	90	5/2+	Differential	Detailed	Kakuee
^{23}Na	(p,p´γ) (p,α´γ)	1636 1634	1-2.9	90	7/2+ 2+	Differential	Detailed	Kakuee
^{23}Na	(p,p´γ)	440	3-4	90, 0, 135, 55	5/2+	Differential	Detailed	Chiari
^{23}Na	(p,p´γ) (p,α´γ)	1636 1634	3-4	90, 0, 135, 55	7/2+ 2+	Differential	Detailed	Chiari
^{23}Na	(p,p´γ)	440	2-3	55 (0, 90, 135)	5/2+	Differential	Detailed	Kiss
^{23}Na	(p,p´γ) (p,α´γ)	1636 1634	2-3	55 (0, 90, 135)	7/2+ 2+	Differential	Detailed	Kiss
^{23}Na	(p,p´γ)	440	4-10	135, 90, 55	5/2+	Differential	Detailed	Strivay
^{23}Na	(p,p´γ) (p,α´γ)	1636 1634	4-10	135, 90, 55	7/2+ 2+	Differential	Detailed	Strivay
^{24}Mg	(p,p´γ)	1369	2-6	0, 55, 90,165	2+	Differential	Detailed	Lagoyannis
^{24}Mg	(p,p´γ)	390	1-3	90	3/2+	Differential	Detailed	Kakuee
^{25}Mg	(p,p´γ)	390	1-3	90	3/2+	Differential	Detailed	Kakuee
^{25}Mg	(p,p´γ)	390	2-5.5	0, 55, 90,165	3/2+	Differential	Detailed	Lagoyannis
^{25}Mg	(p,p´γ)	585	2-5.5	0, 55, 90,165	1/2+	Differential	Detailed	Lagoyannis
^{25}Mg	(p,p´γ)	974	1-3	90	3/2+	Differential	Detailed	Kakuee
^{25}Mg	(p,p´γ)	585	1-3	90	1/2+	Differential	Detailed	Kakuee
^{26}Mg	(p,γ)	1014	1-3	90	3/2+	Differential	Detailed	Kakuee
^{27}Al	(p,p´γ)	844	1-3	90	1/2+	Differential	Detailed+sparse points	Kakuee
^{27}Al	(p,p´γ)	844	2.5-4	45, others	1/2+	Differential+ Thick target	Detailed+sparse points	Chiari
^{27}Al	(p,p´γ)	844	2.5-3.	55	1/2+	Differential+ Thick target	Detailed+sparse points	Kiss
^{27}Al	(p,p´γ)	844	3-10	135	1/2+	Differential+ Thick target	Detailed+sparse points	Strivay
^{27}Al	(p,p´γ)	844	2.5-4	55	1/2+	Differential+ Thick target	Detailed+sparse points	Raisanen
^{27}Al	(p,p´γ)	844	2.5-3	90	1/2+	Differential+ Thick target	Detailed+sparse points	Becker
^{27}Al	(p,p´γ)	1014	1-3	90	3/2+	Differential+ Thick target	Detailed+sparse points	Kakuee
^{27}Al	(p,p´γ)	1014	2.5-4	45, others	3/2+	Differential+ Thick target	Detailed+sparse points	Chiari

Isotope	Reaction	γ-ray [keV]	Energy range [MeV]	Angle	Initial State, Jπ	Type of Data	Comments	Assigned to:
^{27}Al	(p,p´γ)	1014	2.5-3.	55	3/2+	Differential+ Thick target	Detailed+sparse points	Kiss
^{27}Al	(p,p´γ)	1014	3-10	135	3/2+	Differential+ Thick target	Detailed+sparse points	Strivay
^{27}Al	(p,p´γ)	1014	2.5-4	55	3/2+	Differential+ Thick target	Detailed+sparse points	Raisanen
^{27}Al	(p,p´γ)	1014	2.5-3	90	3/2+	Differential+ Thick target	Detailed+sparse points	Becker
^{27}Al	(p,γ)	1779	1.5-4	130	2+	Differential+ Thick target	Detailed+sparse points	Pedro de Jesus
^{27}Al	(p,γ)	1779	1-3	90	2+	Differential+ Thick target	Detailed+sparse points	Kakuee
^{27}Al	(p,γ)	1779	2.5-5	45, others	2+	Differential+ Thick target	Detailed+sparse points	Chiari
^{27}Al	(p,γ)	1779	2.5-5	0, 55, 90,165	2+	Differential+ Thick target	Detailed+sparse points	Lagoyannis
^{27}Al	(p,γ)	1779	2.5-3	55	2+	Differential+ Thick target	Detailed+sparse points	Kiss
^{27}Al	(p,γ)	1779	3-6	135	2+	Differential+ Thick target	Detailed+sparse points	Zucchiatti
^{27}Al	(p,γ)	1779	3-10	135	2+	Differential+ Thick target	Detailed+sparse points	Strivay
^{27}Al	(p,γ)	1779	2.5-4	55	2+	Differential+ Thick target	Detailed+sparse points	Raisanen
^{27}Al	(p,γ)	1779	2.5-3	90	2+	Differential+ Thick target	Detailed+sparse points	Becker
^{27}Al	(p,α´γ)	1369	1-3	90	2+	Differential+ Thick target	Detailed+sparse points	Kakuee
^{27}Al	(p,α´γ)	1369	2.5-4	45, others	2+	Differential+ Thick target	Detailed+sparse points	Chiari
^{27}Al	(p,α´γ)	1369	2.5-5	0, 55, 90,165	2+	Differential+ Thick target	Detailed+sparse points	Lagoyannis
^{27}Al	(p,α´γ)	1369	2.5-3	55	2+	Differential+ Thick target	Detailed+sparse points	Kiss
^{27}Al	(p,α´γ)	1369	3-10	135	2+	Differential+ Thick target	Detailed+sparse points	Strivay
^{27}Al	(p,α´γ)	1369	2.5-4	55	2+	Differential+ Thick target	Detailed+sparse points	Raisanen
^{27}Al	(p,α´γ)	1369	2.5-3	90	2+	Differential+ Thick target	Detailed+sparse points	Becker
^{29}Si	(p,p´γ)	1274	1-3	90	3/2+	Differential+ Thick target	Detailed+sparse points	Kakuee
^{29}Si	(p,p´γ)	1274	4-7	55	3/2+	Differential+ Thick target	Detailed+sparse points	Raisanen
^{nat}Si	(p,p´γ)	1274	2.5-4	45	3/2+	Thick target	Sparse points	Chiari
^{nat}Si	(p,p´γ)	1779	2.5-4	45	2+	Thick target	Sparse points	Chiari
^{28}Si	(p,p´γ)	1779	1-3	90	2+	Differential+ Thick target	Detailed+sparse points	Kakuee

Isotope	Reaction	γ-ray [keV]	Energy range [MeV]	Angle	Initial State, Jπ	Type of Data	Comments	Assigned to:
^{31}P	(p,p´γ)	1266	1-3	90	3/2+	Differential+ Thick target	Detailed+sparse points	Kakuee
^{31}P	(p,p´γ)	1266	2-4	130	3/2+	Differential+ Thick target	Detailed+sparse points	Pedro de Jesus
^{32}S	(d,p´γ)	841	1-2	90	1/2+	Differential+ Thick target	Detailed+sparse points	Kakuee
^{35}Cl	(p,p´γ)	1219			1/2+	Literature	Detailed+sparse points	Pedro de Jesus
^{35}Cl	(p,p´γ)	2230			2+	Literature	Detailed+sparse points	Pedro de Jesus
^{35}Cl	(d,p´γ)	1165	1-2	90	1+	Differential+ Thick target	Detailed+sparse points	Kakuee
^{53}Cr	(p,γ)	62.3/90.6	1-3	90		Differential	Detailed	Goncharov
^{54}Cr	(p,nγ)	62.3/90.6	1.5-3	90		Differential	Detailed	Goncharov

Table 4.3. Responsible per Element/Isotope

Reactions Related to Element/Isotope	**Responsible Person**
Li	Chiari
B	Lagoyannis
Be	Strivay
^{12}C	Becker
N	Kiss
F	Zucchiatti
Na	Bogdanovic Radovic
Mg	Kakuee
Al	Pedro de Jesus
Si	Raisanen
P	Pedro de Jesus
Cl	Pedro de Jesus
S	Lagoyannis
Ti	Goncharov
Cr	Goncharov

Table 4.4. Special actions

Action on	Subject
All concerned	Send to Daniel in a few weeks the results of the efficiency calibration of the γ-ray detector and the details of the experimental set-up.
All concerned	Perform over the period of the CRP the remaining assigned measurements indicated in Table 4.1.
All concerned	Production and distribution of targets for the remaining measurements.
All concerned	For inter-laboratory comparison make both the thin and thick aluminium measurements, and send the results to Adelaide till the end of February 2013.
Gurbich	Complete the necessary changes in IBANDL to display PIGE data.
Pedro de Jesus	Distribute the ERYA code to the participants including a comprehensive manual in English.
Pedro de Jesus	In a second step upgrade the ERYA code in order to handle depth profiling.
Becker, Lagoyannis	Find out the information of cross sections relevant to PIGE in the astrophysics community resources and input them in IBANDL.
Responsible Persons (Table 4.2)	Collect the data from literature, compile it in the R33 format and sent it to Alex to be included in IBANDL.
Responsible Persons (Table 4.2)	Submit assessment of those reactions assigned in Table 4.1 paying attention in retrieving angular distributions wherever available.
Responsible Persons (Table 4.2)	Collect the data measured by all the groups involved in a set of experiments, make a comparison, suggest eventual correction actions.
All concerned	Prepare an abstract (deadline 15th April) and a paper to submit to ECAART.
Semkova	On request of participants, digitize data for inclusion in IBANDL and EXFOR.

5. Conclusions

The Second Research Coordination Meeting (RCM) on the Development of a Reference Database for Particle-Induced Gamma ray Emission (PIGE) Spectroscopy was held at the IAEA, Vienna from 8-12 October 2012.

Participants presented the work that has been done so far, and certain aspects of the methodology adopted in the first RCM were revisited, such as accelerator calibration, target preparation and γ-ray detector efficiency calibration. Regarding the production of the remaining experimental data, participants agreed that their priority should be to carry out an inter-laboratory comparison of thin and thick aluminium measurements in order to deal with possible sources of discrepancies and systematic errors. Each participant assumed the responsibility for coordinating a set of measurements on a particular nuclide, and also for reviewing the scientific literature in search of previous data, and assessing the data before submitting them for inclusion in IBANDL. The preliminary versions of the computer codes that would allow the final user to profit from the PIGE database were presented and the feasibility of performing evaluations and theoretical calculations was highlighted. Until the next and final meeting, foreseen for the second quarter of 2014, the CRP webpage will serve as a forum for communication and information of the participants' progress with their individual assignments.

Annex A

2nd Research Coordination Meeting on
Development of a Reference Database for PIGE Spectroscopy

IAEA Headquarters, Vienna, Austria
8 – 12 October 2012
Meeting Room A0531

Preliminary AGENDA

Monday, 8 October

08:30 – 09:30 **Registration (IAEA Registration Desk, Gate 1)**

09:30 – 10:15 **Opening Session**
Opening Remarks and Welcome (R.A. Forrest, SH-NDS)
Introduction: Objectives of this RCM (D. Abriola)
Election of Chairman and Rapporteur
Discussion and Adoption of the Agenda (Chairman)

10:15 – 10:45 *Coffee break*

10:45 – 12:15 **Presentations**

1) ***Calibration and thick and thin Al(p,g) and (p,p'g) cross sections***
Pedro de Jesus (~ 30 min)
2) ***Gamma ray production cross-sections from deuteron induced nuclear reaction measurements***
Kiss (~ 30 min)
3) ***Measurements and literature survey of some (p,γ) and (p,αγ) reactions important for ion beam analysis***
Becker (~ 30 min)

Coffee break as needed

12:15 – 12:30 *Administrative matters*

12:30 – 14:00 *LUNCH*

14:00 – 17:30 **Presentations (cont'd)**

4) ***Differential cross section measurements of the $^{32}S(p,p'g)^{32}S$ reaction***
Lagoyannis (~30 min)
5) ***Differential cross sections for the $^{14}N(p,p'\gamma)^{14}N$, $^{28}Si(p,p'\gamma)^{28}Si$ and $^{29}Si(p,p'\gamma)^{29}Si$ reactions***
Raisanen (~30 min)
6) ***Setting up the HPGe array for PIGE cross-section measurements at LABEC***
Chiari (~20 min)
7) ***PIGE measurements at the Rudjer Boskovic Institute***
Bogdanović Radović (~30 min)

Round table discussion

Coffee break as needed

Tuesday, 9 October

09:00 – 12:30 **Presentations (cont'd)**

8) ***IBA reaction chamber developed for PIGE analysis***
Kakuee (~30 min)

9) ***Accelerator calibration and measurement of gamma production in thin Al targets at CMAM***
Zucchiatti (~30 min)

10) ***PIGE-setup and measurements at IPNAS laboratory***
Strivay (~30 min)

11) ***Measurement of excitation yields of low energy prompt γ-ray from proton bombardment of Ti-foils with energies ranging between 1.0 and 3.0 MeV***
Utyenkov (~30 min)

12) ***Changes in the R33-format and modification of IBANDL to accommodate PIGE data*** (~15 min)
Study of the feasibility of producing evaluations for PIGE (~15 min)
Gurbich

Round table discussion

Coffee break as needed

12:30 – 14:00 *LUNCH*

14:00 – 17:30 **Methodology (discussion)**

1) Database format and data issues

Coffee break as needed

Wednesday, 10 October

09:00 – 09:30 ***Present version of ERYA code***
Pedro de Jesus

09:30 – 12:30 **Methodology (discussion cont'd)**

2) Evaluation: codes and methods
3) Benchmarks: codes and methods

Coffee break as needed

12:30 – 14:00 *LUNCH*

14:00 – 17:30 **Methodology (discussion cont'd)**

4) End user: application software

Coffee break as needed

19:00 ***DINNER at a restaurant in the city***
("Gastwirtschaft Huth", see separate information)

Thursday, 11 October

09:00 – 12:30	**Round Table**
	Coffee break as needed
12:30 – 14:00	*LUNCH*
14:00 – 17:30	**Drafting of the 2nd RCM Summary Report**
	Coffee break as needed

Friday, 12 October

09:00 – 12:30	**Drafting of the 2nd RCM Summary Report (cont'd)**
	Coffee break as needed
12:30 – 14:00	*LUNCH*
14:00 – 16:00	**Closing of the Meeting**

Annex B

2nd Research Coordination Meeting on
"Development of a Reference Database for PIGE Spectroscopy"
IAEA, Vienna, Austria
8 – 12 October 2012

LIST OF PARTICIPANTS

BELGIUM

David Strivay
Institut de Physique Nucleaire
Atomique et de Spectroscopie
Universite de Liège
Sart Tilman B15
4000 Liège
Tel: +
E-mail: dstrivay@ulg.ac.be

CROATIA

Iva Bogdanovic Radovic
Department of Experimental Physics
Institute Ruder Boskovic
Bijenicka cesta 54
10000 Zagreb
Tel: +385-1-4571-227
E-mail: iva@irb.hr

FINLAND

Jyrki Raisanen
Division of Materials Physics
Department of Physics
Siltavuorenpenger 20D
00014 Helsinki
Tel: +358 9 191 50082
E-mail: jyrki.raisanen@helsinki.fi
raisanen@mappi.helsinki.fi

GERMANY

Hans-Werner Becker
Ruhr Universität Bochum
Gebäude NT05/130
Postfach 102148
Bochum 44721
Tel: +49 234 3223607
E-mail: hans-werner.becker@rub.de

GREECE

Anastasios Lagoyannis
National Center of Scientific Research
"Demokritos"
Agia Paraskevi
P.O. Box 60228
15310 Athens
Tel: +302106503597
E-mail: lagoya@inp.demokritos.gr

HUNGARY

Arpad Zoltan Kiss
Hungarian Academy of Sciences
Bem ter 18/c
PO Box 51
4001 Debrecen
Tel: + 36 52 509200
E-mail: azkiss@namafia.atomki.hu

IRAN

Omidreza Kakuee
Nuclear Science and Technology
Research Institute
End of North Karegar Ave.
PO Box 14395-836
Tehran
Tel: + 98(0)21-82063213
E-mail: okakuee@aeoi.org.ir

ITALY

Massimo Chiari
Istituto Nazionale di Fisica Nucleare
Via Sansone 1
Sesto Fiorentino
50019 Firenze
Tel: +39-055-457-2273
E-mail: chiari@fi.infn.it

PORTUGAL

Adelaide Pedro de Jesus
Centro de Física Nuclear
Av. Gama Pinto, N˚2
1649-003 Lisboa
Tel: + 351 21 790 4975
E-mail: ajesus@fct.unl.pt

SPAIN

Alessandro Zucchiatti
Centro Micro-Análisis de Materiales
Universidad Autónoma de Madrid
C/ Faraday 3, Campus de Cantoblanco
Madrid 28049
Tel: +34 91 497 2791
E-mail: alessandro.zucchiatti@uam.es

UKRAINE

Sergiy Utyenkov
Kharkov Institute of Physics and Technology
National Science Center Kharkov Institute
of Physics & Technology
Akademicheskaya Str.1
Kharkov 61108
Tel: +
E-mail: Utenkov@i.ua

CONSULTANT

Alexander Gurbich
Institute of Physics and Power
Engineering
Bondarenko Square, 1
249033 Obninsk, Kaluga Region
RUSSIA
Tel: +7 48439 94169
E-mail: gurbich@ippe.ru

IAEA

Daniel Abriola
International Atomic Energy Agency
(IAEA)
Nuclear Data Section
Division of Physical and Chemical
Sciences
Wagramer Strasse 5
1400 Vienna
Tel. +43-1-2600 21712
Fax +43-1-2600 7
E-mail: d.abriola@iaea.org

Paraskevi (Vivian) Dimitriou
International Atomic Energy Agency
(IAEA)
Nuclear Data Section
Division of Physical and Chemical
Sciences
Wagramer Strasse 5
1400 Vienna
Tel. +43-1-2600 21708
Fax +43-1-2600 7
E-mail: p.dimitriou@iaea.org

Nuclear Data Section
International Atomic Energy Agency
Vienna International Centre, P.O. Box 100
A-1400 Vienna
Austria

e-mail: services@iaeand.iaea.org
fax: (43-1) 26007
telephone: (43-1) 2600-21710
Web: http://www-nds.iaea.org